ERRORS IN SKIN TEMPERATURE MEASUREMENTS

Murielle Dugay

Thesis Prepared for the Degree of

MASTER OF SCIENCE

UNIVERSITY OF NORTH TEXAS

December 2008

APPROVED:

Sandra Boetcher, Major Professor
Matthew J. Traum, Committee Member
Nourredine Boubekri, Committee Member and
Interim Chair of the Department of
Mechanical and Energy Engineering
Costas Tsatsoulis, Dean of the College of
Engineering
Sandra L. Terrell, Dean of the Robert B. Toulouse
School of Graduate Studies

Dugay, Murielle. Errors in skin temperature measurements. Master of Science (Mechanical and Energy Engineering), December 2008, 67 pp., 3 tables, 62 illustrations, references, 24 titles.

Numerical simulation is used to investigate the accuracy of a direct-contact device for measuring skin-surface temperature. A variation of thermal conductivity of the foam has greater effect on the error rather than a variation of the blood perfusion rate. For a thermal conductivity of zero, an error of 1.5 ^{o}C in temperature was identified. For foam pad conductivities of 0.03 and 0.06 W/m-^{o}C, the errors are 0.5 and 0.15 ^{o}C. For the transient study, with k=0 W/m-^{o}C, it takes 4,900 seconds for the temperature to reach steady state compared with k=0.03 W/m-^{o}C and k=0.06 W/m-^{o}C where it takes 3,000 seconds. The configuration without the foam and in presence of an air gap between the skin surface and the sensor gives the most uniform temperature profile.

ACKNOWLEDGMENTS

I would first like to thank Dr. Sandra Boetcher for her great help and encouragement during all of the steps of the thesis. I acknowledge Dr. Boetcher for being an inspiration and for her confidence at every moment. She also permitted me to reach the main goals of the present study within the deadlines.

I gratefully acknowledge Professor Ephraim M. Sparrow from the University of Minnesota for his contribution throughout the study. It was an honor for me to be able to work on a research project under the guidance of such an eminent professor in the mechanical engineering field.

Thanks also to the faculty and staff in the department of Mechanical and Energy Engineering of the University of North Texas for providing me with useful advice as well as software and computational materials.

My thanks also go to my friend, Emmanuel Lewis Jr., who showed a tremendous amount of support during the past two years. I sincerely thank him for being there whenever I needed him. Last but not least, I am grateful to my parents for supporting me in whatever I wished to do, no matter how far I chose to study, and for being a never ending source of inspiration.

TABLE OF CONTENTS

LIST OF TABLES

LIST OF FIGURES

CHAPTER 1

INTRODUCTION

1.1 Engineering in Medicine

Biomedical engineering is a dynamic and fast expanding field in which major advances in biomedical research and medicine are made. The combination of biomedical science together with engineering and physics has the capacity to generate powerful techniques and tools to solve current medical issues. Engineering in medicine involves several areas of expertise such as mechanics, controls, electrical engineering, materials science, as well as fluids and heat transfer. The present study focuses on computational heat transfer analysis which is applied here to the human physiology. Human physiology is the science of the physical, mechanical and chemical functions of the organs and the cells of the healthy human body.

1.2 Core Body Temperature

Temperature in the body is affected by both the environment outside of a human and by the amount of heat generated by anabolic reactions within the body which are regulated by respiratory and cardiovascular systems. Core body temperature, which is the operating temperature of a human, is defined in deep structures of the body as opposed to temperatures of peripheral tissues.

Temperature examination in the rectum instead of oral temperature is the traditional measurement used to estimate core body temperature. The drop of the core body temperature can result in hypothermia which can lead to death.

Human body temperature depends upon the location in the body where the measurement is made. Besides the dependency upon position, there is usually some natural variation in body temperature with the time of day and upon the body conditions. Thermoregulation keeps the human body operating at optimal temperature by controlling the rate of chemical reactions so that the body stays at a temperature of 36.8 °C. Taking the temperature of a patient is an initial part of a full clinical examination.

1.2.1 Methods of Temperature Measurement

Several indirect measurement methods are used because direct measurement of core body temperature would require invasive insertion of a probe and is not usually possible in a clinical setting. The rectal temperature is considered to give the most accurate assessment of core body temperature. However, its recording is not appreciated by patients and medical staff.

Color-changing plastic thermometer strips can be placed on the forehead; however, they don't give an accurate reading because the ambient air temperature interferes with the reading. Recording the temperature under the armpit with a thermometer is a better way to measure temperature because this method is less affected by surrounding air temperature. However, the measured temperature is still eager to diverge from true core temperature if there are variations in blood circulation.

1.3 Mean Body Temperature

The mean body temperature (MBT) is a well-established indicator that is widely used to assess the thermal status of the body. Also, it serves as a means of judging the efficacy of thermal therapies. For instance, the MBT is used to assess the absence or presence of both hypothermia and hyperthermia which can quickly and dramatically impact the good health of the patient.

1.3.1 Measurement of the Mean Body Temperature

The MBT is obtained by combining temperatures measured at various locations within and on the surface of the body rather than determined by direct measurement. There exists a large amount of proposed methods for determining the MBT from component temperatures [1 – 11]. The currently accepted approach is to use the following formula

$$MBT = \alpha\, T_{core} + (1 - \alpha)\overline{T_{skin}} \tag{1.1}$$

In this equation, the core temperature is determined by an esophageal thermal sensor which is partially invasive but is removed after the measurement is made. The mean skin temperature is evaluated by measuring the skin surface temperature at numerous locations on the surface. Thus, the importance of skin-surface temperature measurements in the determination of the mean body temperature is demonstrated. The contemporary literature suggests values of the weighting constant α between 0.1 and 0.4 [8, 9]. The

size of this range is sufficiently large to create considerable uncertainties in the determination of the MBT.

Mean body temperature is, in term of use, a measure of the thermal energy possessed by the body. However, the definition of the MBT conveyed by Eq. (1.1) is not an indicator of thermal energy.

A more logical approach to the determination of the MBT was proposed [12]. The implementation of the new approach is as follows. First, a number of distinct zones of the body, each of mass M_j, may be selected. For example, zone 1 may be the trunk and head, zone 2 the thighs, 3 the legs, 4 the feet, 5 the upper arms, 6 the lower arms, and 7 the hands. If N zones are chosen, the index j ranges from 1 to N. Let the temperature of each zone be denoted by T_j. Then, a rational definition of the MBT follows as

$$MBT = \left[\sum_{j=1}^{N}\left(M_j \times T_j\right)\right] / \sum_{j=1}^{N} M_j \tag{1.2}$$

1.4 Errors in Skin-surface Temperature Measuring Devices

As alluded to above, knowledge of the skin-surface temperature serves as a clinical diagnostic metric. Among the various modalities for measuring skin-surface temperature, clinicians prefer the use of direct-contact devices. Those devices usually include a miniature thermocouple or thermistor as the sensing element. The sensing element is threaded into a layered assembly which consists of a thin band-aid-like strip of plastic backed by a layer of compliant foam. The plastic strip is adhesive coated on both

of its faces. One face of the strip is affixed to the skin surface, while the other face is adhered to the foam backing. In another manifestation, the plastic strip is replaced with a thin metal foil which serves as a heat spreader. Such devices are commercially available under brand names such as Mon-a-therm (Nellcor, Pleasanton, CA successor to Mallinckrodt Medical, St. Louis, MO) and Vital Sense (Bend, OR).

In term of accuracy of the temperature measurement, the presence of the foam backing layer in those devices is a source of concern. The foam as a thermal resistance tends to block the heat flow from the skin surface to the ambient, thus elevating the surface temperature above its value in the absence of the blockage. As a matter of fact, the recognition that blockage of skin-surface heat flow elevates skin-surface temperature has been used as the basis of a device to measure deep-tissue temperature [13-20].
It is of interest that any in-depth investigation of the potential errors inherent in direct-contact of foam-backed temperature sensors appears not to have been published. The only somewhat relevant work is confined to experimental comparisons of direct-contact devices with other modalities of skin temperature measurement, without discussion of the insulating role of the foam [21-23].

First, a steady state-study of errors in skin temperature measurements with such an instrument device is presented. Then, in a third chapter, a transient study of skin-surface temperature errors is discussed. Finally, the effect of contact resistance will be examined.

1.5 Nomenclature

c	specific heat [J/kg-^{o}C]
h	heat transfer coefficient [W/m^2-^{o}C]
k	thermal conductivity [W/m-^{o}C]
M	mass
N	number of zones
n	surface norma
t	time [s]
T	temperature [^{o}C]
r, z	cylindrical coordinates [mm]
ρ	density [kg/m^3]
ω	blood perfusion [(m^3/s)/m^3]

Subscripts

b	blood
c	core
i	initial
j	index
α	weighting constant
∞	ambient

CHAPTER 2

STEADY STATE

2.1 Introduction

In the present chapter, a numerical steady-state simulation of the temperature distribution and heat flow in human skin and tissue beneath a skin-surface temperature measuring device is performed. The multi-dimensional bioheat equation is used as the analysis tool. Parametric variations of the key variables are performed to strengthen the validity of the extracted conclusions.

2.2 Physical Model

The sub-skin human anatomy varies with location over the body. In the present study, a simple model will be used to investigate the accuracy of skin-surface temperature measurements by means of the clinically standard devices described earlier. The model, displayed in Fig. 2.1, consists of three layers: skin, fat, and muscle. At the bottom, the muscle layer interfaces with the body core. Also shown in the figure is the modeled skin-surface temperature measurement device. It consists of a very thin copper sheet, which serves as a heat spreader, topped with a foam pad. Not shown in the diagram is a miniature thermistor or thermocouple, situated at the interface of the pad and the heat thermocouple, which serves as the temperature sensor. All indicated dimensions are in millimeters and are illustrated in Fig. 2.1.

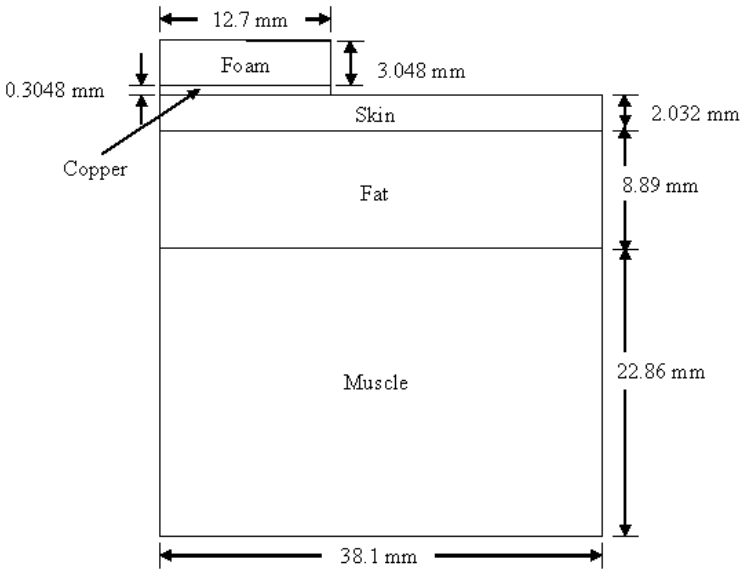

Fig. 2.1 Schematic diagram of an axisymmetric view of the foam and copper spreader placed onto a section of skin, fat, and muscle.

The geometry is a radial slice whose left-hand vertical edge is the axis of symmetry. The width of the assembly defines the space in which the temperature and heat flow are expected to be affected by the presence of the measurement device. As will be shown later, a larger solution domain was tested and it was determined that a radial slide of width 38.1 mm was an adequate width for the solution domain.

At the exposed surfaces of the skin and of the temperature measurement device, heat loss by convection to the ambient air and by radiation to surrounding solid objects is taken into account in the simulation. The lower surface of the muscle layer is taken to be

at the body temperature (37 ^{o}C). The right-hand vertical boundary of the solution space, situated beyond the reach of the disturbance caused by the measuring device, is considered adiabatic.

2.3 Analysis

The analysis to be performed here seeks to determine the error in the steady-state temperature measurement, and the selected analysis tool is the well-known Pennes bioheat equation [24]. A survey of the recent bioheat literature has established that it is virtually the only bioheat equation in present use.

The axisymmetric form of the steady-state Pennes bioheat equation is

$$k\left[\frac{1}{r}\frac{\partial}{\partial r}\left(r\frac{\partial T}{\partial r}\right)+\frac{\partial^2 T}{\partial z^2}\right]+\omega_b\rho_b c_b(T-T_c)=0 \qquad (2.1)$$

This equation has to be applied differently in the skin, fat, and muscle layers. Consequently, the property k pertains to the thermal conductivity of the tissue in the respective layers. The other properties, ρ_b the density and c_b the specific heat capacity pertain to blood and are common to all of the body layers. The quantity ω_b is the blood perfusion rate and has units of m^3/s per m^3 of tissue. Of all of the inputs that must be provided for the solution of Eq. (2.1), it is the most uncertain. In light of this, ω_b was varied parametrically over a range of reasonable values. The temperature T represents the local tissue temperature, and T_c is the body core temperature. The metabolic heat generation has not been included in Eq. (2.1) because it is small compared with the perfusion term.

Heat conduction in the metallic heat spreader and in the foam pad is governed by Laplace's equation,

$$\frac{1}{\mathrm{r}}\frac{\partial}{\partial \mathrm{r}}\left(\mathrm{r}\frac{\partial \mathrm{T}}{\partial \mathrm{r}}\right)+\frac{\partial^2 \mathrm{T}}{\partial \mathrm{z}^2}=0 \tag{2.2}$$

Although the thermal conductivity is absent from Eq. (2.2), it still must be specified because it appears both in the boundary conditions and in the interface continuity conditions.

Attention will now be turned to the boundary and continuity conditions. At the exposed surfaces of the skin and the temperature measurement device, the heat convection is governed by the following equation,

$$-\mathrm{k}\left(\frac{\partial \mathrm{T}}{\partial \mathrm{n}}\right)=\mathrm{h}(\mathrm{T}-\mathrm{T}_{\infty}) \tag{2.3}$$

where n is the surface normal. The conductivity is that of the skin, the foam, or the copper, h is the combined convective and radiative heat transfer coefficients, and T_∞ is the temperature of the ambient air and the surrounding solid objects. The following values are used, h = 13.63 W/m^2-^{o}C and T_∞ = 22 ^{o}C. The boundary conditions are illustrated in Fig. 2.2.

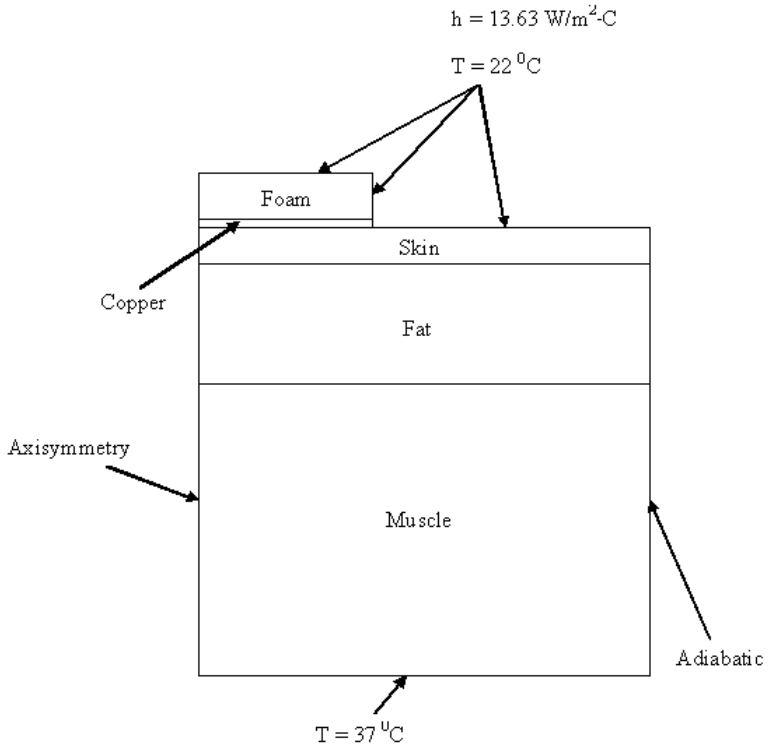

Fig. 2.2 Schematic diagram illustrating the boundary conditions.

Continuity of temperature and heat flux is required at the interfaces of the layers. As already noted, the right-hand side of the surface of the solution space is adiabatic, and the temperature of the bottom of the muscle layer is at 37 ^{o}C. Also, T_c in Eq. (2.1) is taken to be 37 ^{o}C.

Table 2.1 shows the thermophysical properties of the five materials. The values of the thermal conductivity of the foam and the blood perfusion rate of the skin, fat, and muscle were varied parametrically to test the sensitivity of the values to the solution of the problem.

Table 2.1 Material properties used in the simulation.

	k [W/m-^{o}C]	$\rho_b c_b$ [J/m^3-^{o}C]	ω_b [(m^3/s)/m^3]
Skin	0.62	4×10^6	0, 0.001, 0.003, 0.005
Fat	0.48		
Muscle	1.26		
Foam	0, 0.03, 0.06		
Copper	380.51		

The numerical simulations were performed using ANSYS 11.0 finite element software. For the mesh, an adequate element type was chosen to be quad 4 node 55. The number of nodes used in the execution of the solution was 118,000 (Fig. 2.3(a)). A mesh-independence study was conducted to verify the accuracy of the solution. The number of nodes was doubled to 236,000 (Fig. 2.3(b)) and the error in temperature values was equal to 0.02% as illustrated in Fig. 2.4.

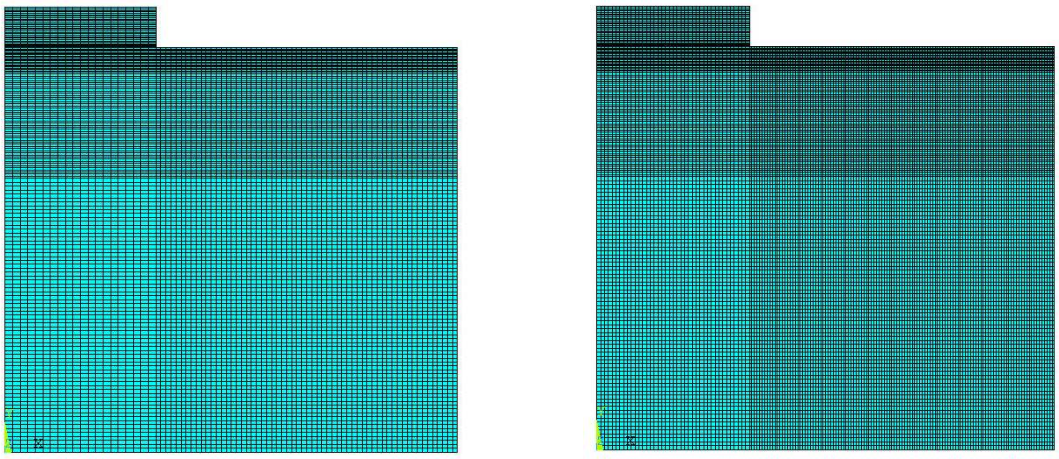

(a) (b)

Fig. 2.3 Diagram of the mesh with (a) 118,000 nodes, and (b) 236,000 nodes.

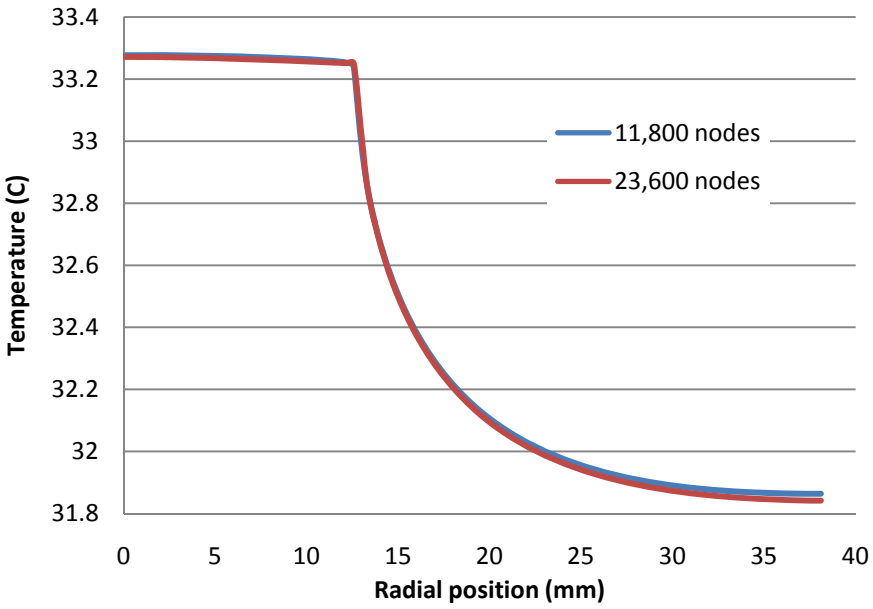

Fig. 2.4 Skin-surface temperature plotted as a function of radial distance for two different meshes for k = 0 W/m-C and $\omega = 0.005\ s^{-1}$.

2.4 Results and Discussion

The result of most immediate practical relevance is the measured skin-surface temperature and its deviation from the actual skin-surface temperature. This information is conveyed in Figs. 2.5, 2.6, and 2.7, respectively for values of the thermal conductivity of the foam insulation pad of 0, 0.03, and 0.06 W/m-^{o}C. The $k = 0$ value corresponds to an upper bound of the possible temperature measurement error.

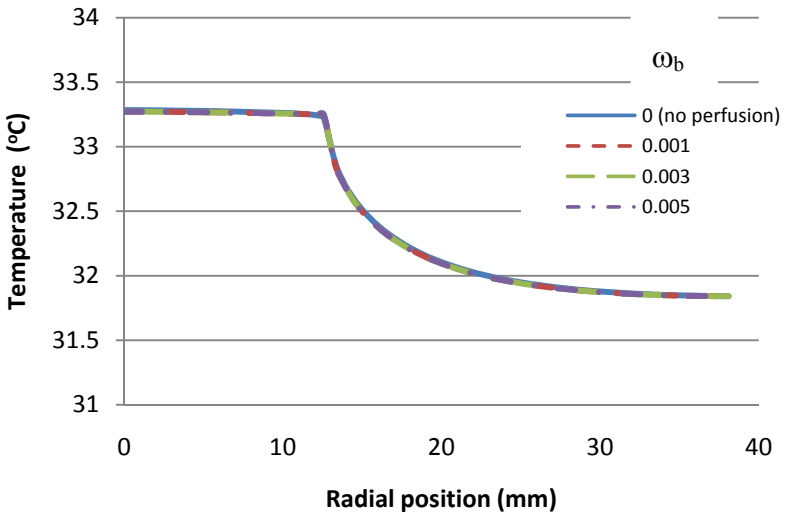

Fig. 2.5 Skin-surface temperature plotted as a function of radial distance for several values of blood perfusion for k = 0 W/m-^{o}C.

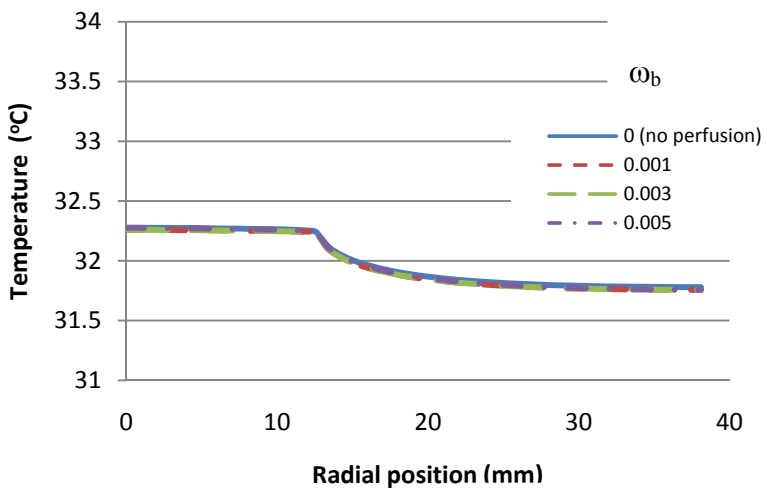

Fig. 2.6 Skin-surface temperature plotted as a function of radial distance for several values of blood perfusion for k = 0.03 W/m-^{o}C.

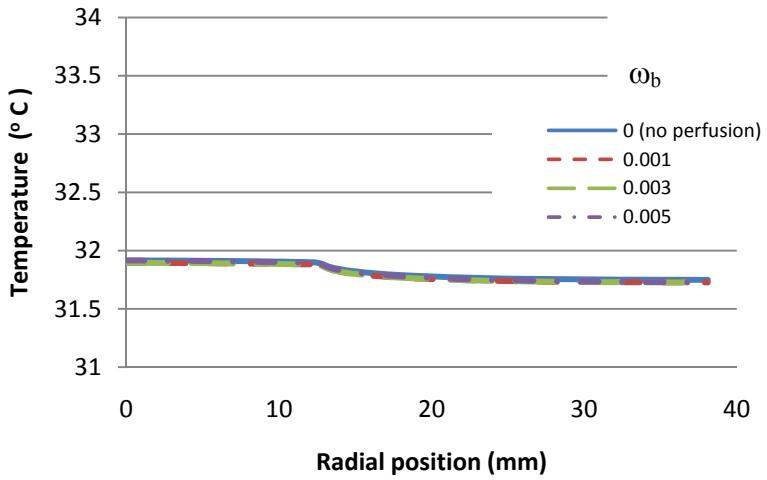

Fig. 2.7 Skin-surface temperature plotted as a function of radial distance for several values of blood perfusion for k = 0.06 W/m-^{o}C.

In each figure, the skin-surface temperature is plotted as a function of the lateral distance measured along the skin from the symmetric axis of the device. The plateau in the temperature distribution corresponds to skin surface locations situated beneath the measurement device, and the outboard end of the temperature distribution corresponds to the true skin temperature.

The upper bound of the temperature measurement error as shown in Fig. 2.5 is found to be about 1.5 ^{o}C. Actual measurement errors of this magnitude would be unacceptable. A more-realistic upper bound, corresponding to k = 0.03 W/m-^{o}C, shown in Fig. 2.6 is 0.5 ^{o}C. This level of accuracy may be regarded as acceptable for non-critical situations. The case of k = 0.06 W/m-^{o}C, displayed in Fig. 2.7, pertains to foams of medium insulation capability. The temperature error of 0.15 ^{o}C for this case may be regarded as acceptable.

The results exhibited in Figs. 2.5, 2.6, and 2.7 encompass values of the volumetric blood perfusion rate of 0, 0.001, 0.003, and 0.005 (m^3/s)/m^3. It is evident from the figures that blood perfusion in this range does not affect the results. Figure 2.8 shows a comparison of the data for all of the parametric cases.

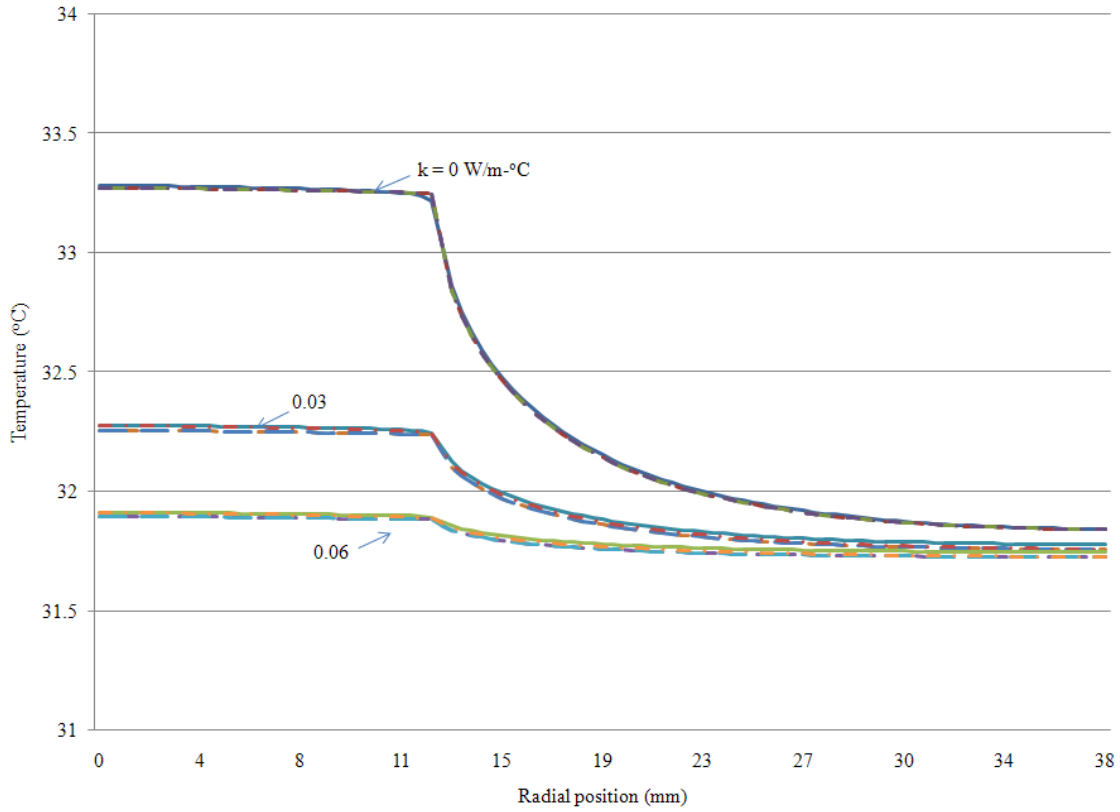

Fig. 2.8 Temperature profile versus the skin surface for all of the different perfusion cases.

2.4.1 Temperature Contour Diagrams

Temperature contour diagrams are presented in Figs. 2.9, 2.10, and 2.11, respectively for cases where k = 0, 0.3, and 0.6 W/m-^{o}C. For specificity, the volumetric perfusion rate is chosen as 0.003 (m^3/s)/m^3 for these figures. To aid in the evaluation of the results, it may be noted that in the absence of the skin temperature measurement device, the isotherms would be perfectly straight and horizontal. Also as a further aid to clarity, the boundaries of the several layers that make up the solution space are shown in the figures as thin horizontal lines.

In Fig. 2.9, it is shown that in the presence of the measurement device with a perfectly insulating foam pad ($k = 0$), there is a disruption of the isotherms. In particular, the isotherms are elevated in the space beneath the measurement device. For the case of k = 0.03 W/m-^{o}C (Fig. 2.10), the isotherms directly underneath the device continue to be elevated, but the elevation decays at greater depths beneath the device. For the least-insulating foam considered here, k = 0.06 W/m-^{o}C, the departure of the isotherms from an array of straight, horizontal lines is confined to the skin layer (Fig. 2.11).

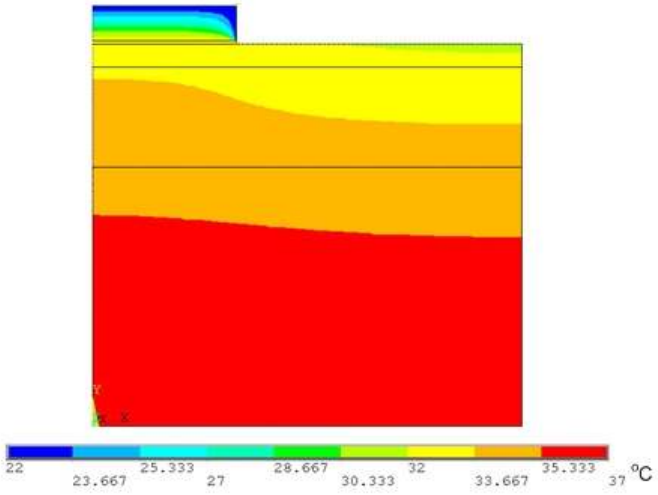

Fig. 2.9 Temperature contour diagram for k = 0 W/m-^{o}C and ω_b = 0.003 (m^3/s)/m^3.

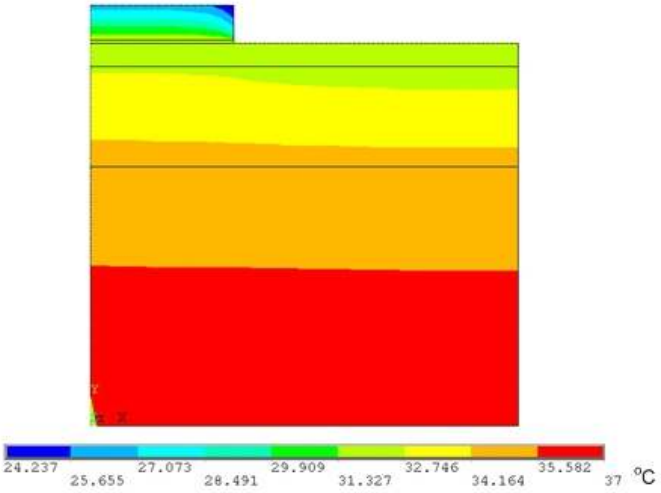

Fig. 2.10 Temperature contour diagram for k = 0.03 W/m-^{o}C and ω_b = 0.003 (m^3/s)/m^3.

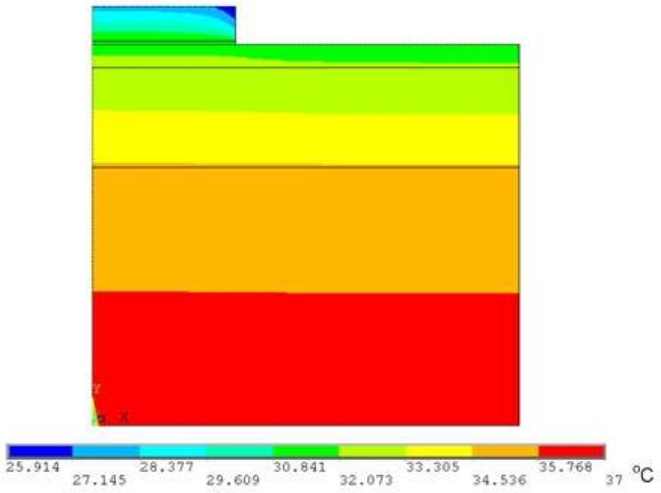

Fig. 2.11 Temperature contour diagram for k = 0.06 W/m-^{o}C and ω_b = 0.003 (m^3/s)/m^3.

Several different widths for the solution domain were examined. The width of the domain of study was determined such as the lateral space was no longer affected by the presence of the measurement device. The sufficiency of the width as bounding the

affected region in term of temperature and heat flow was checked during the numerical study. Figures 2.12 - 2.15 are the temperature contour diagrams for a thermal conductivity of the foam pad equal to zero and with a far-field boundary chosen to be at a radial distance of 114.3 mm. As illustrated in the following figures, the isotherms stay straight and horizontal after the previously used right far-field boundary value of $r = 38.1$ mm.

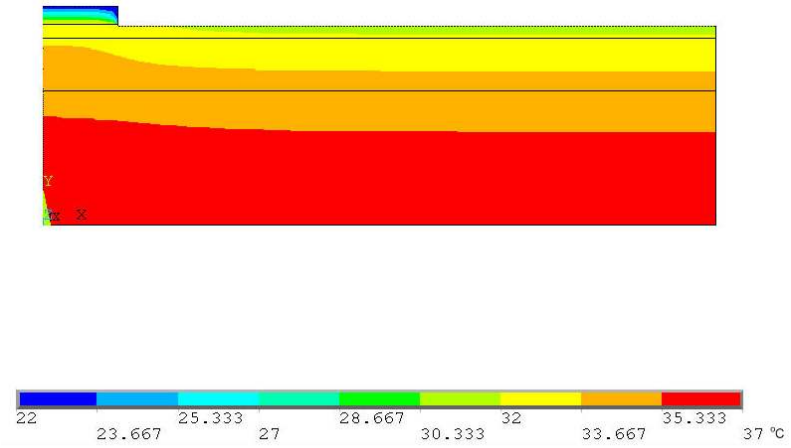

Fig. 2.12 Temperature contour diagram for k = 0 W/m-^{o}C and $\omega_b = 0$ (m^3/s)/m^3.

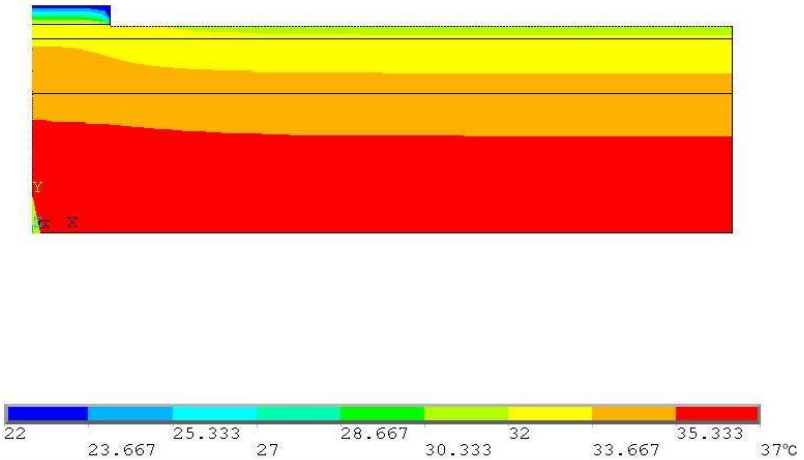

Fig. 2.13 Temperature contour diagram for k = 0 W/m-^{o}C and $\omega_b = 0.001$ (m^3/s)/m^3.

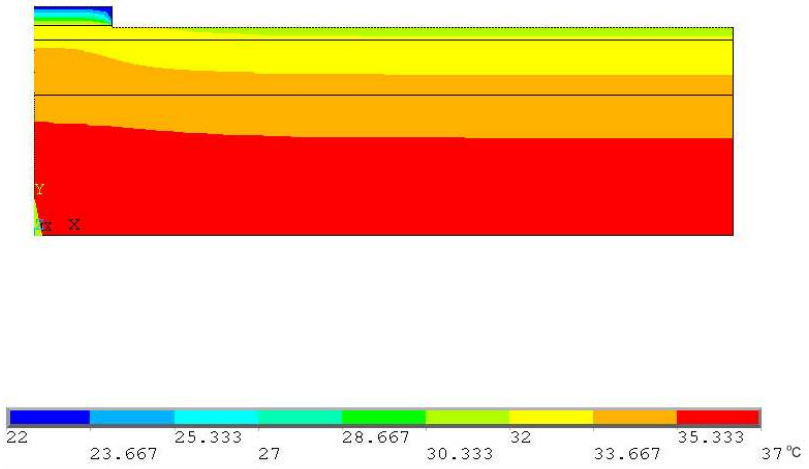

Fig. 2.14 Temperature contour diagram for k = 0 W/m-^{o}C and ω_b = 0.003 (m^3/s)/m^3.

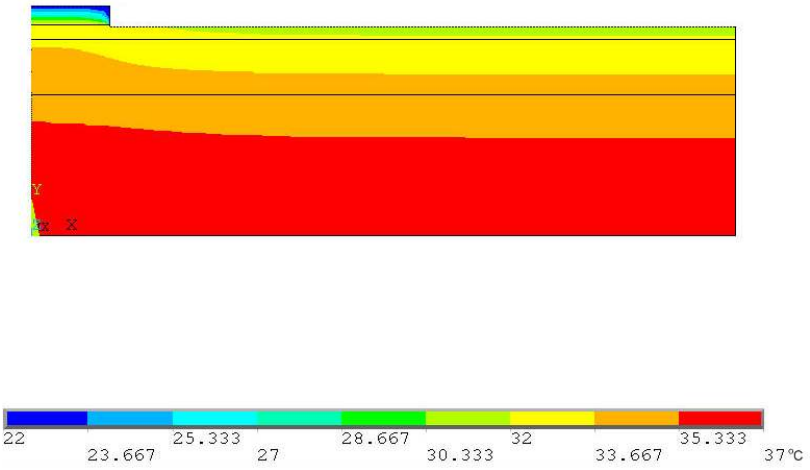

Fig. 2.15 Temperature contour diagram for k = 0 W/m-^{o}C and ω_b = 0.005 (m^3/s)/m^3.

The sufficiency of the width of 38.1 mm as the far-field boundary is also demonstrated in the skin-surface temperature profile of Figure 2.16.

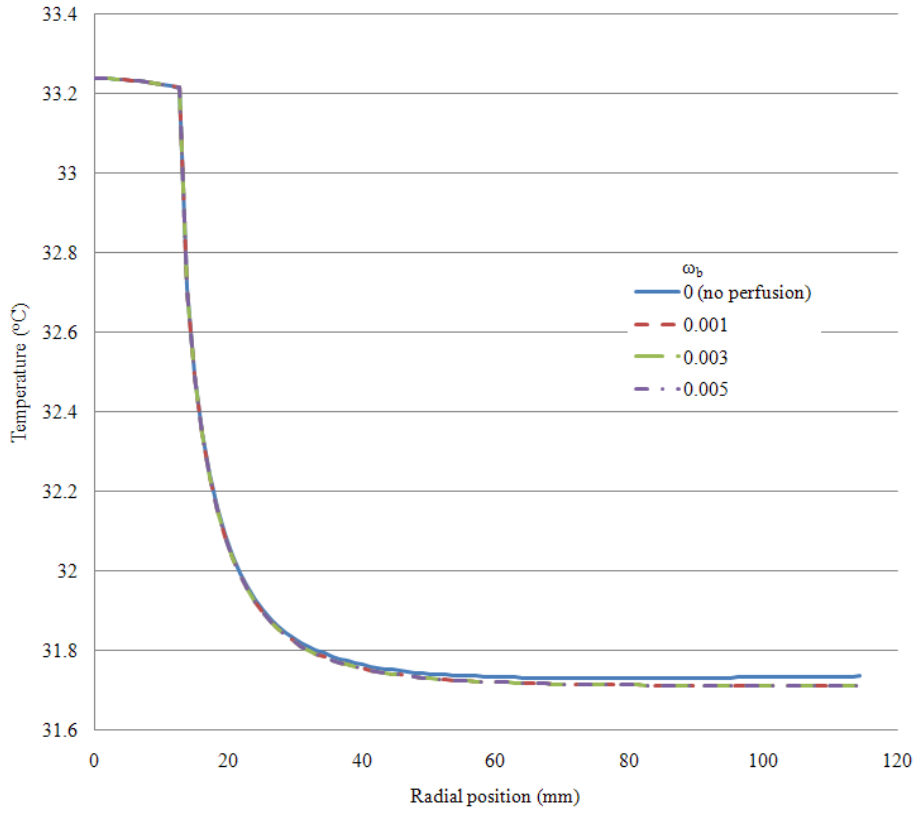

Fig. 2.16 Temperature profile at the skin surface with an extended solution domain.

The temperature contour diagrams conveyed in Figs. 2.17- 2.25 encompass values of the volumetric blood perfusion rate of 0, 0.001, 0.003 and 0.005 $(m^3/s)/m^3$ for different values of the thermal conductivity of the foam. As shown in those figures, for a given value of thermal conductivity of the foam pad, the temperature contour diagrams are essentially the same for different values of the blood perfusion rate.

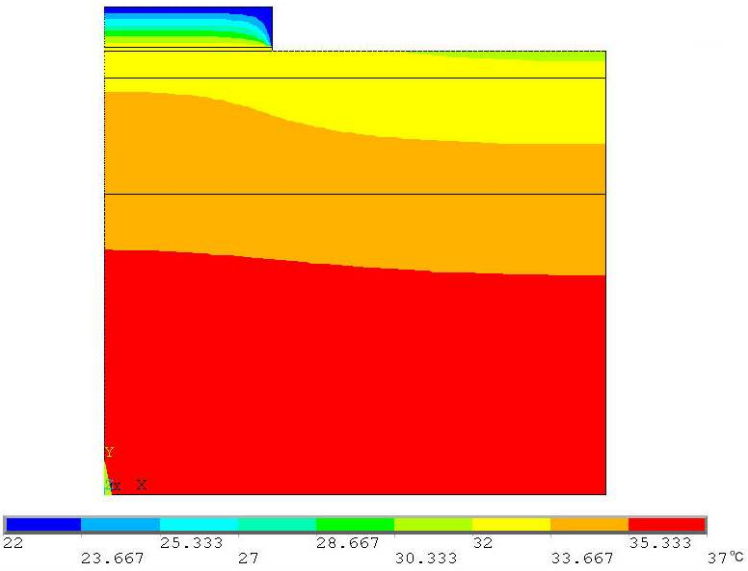

Fig. 2.17 Temperature contour diagram for k = 0 W/m-^{o}C and ω_b = 0 (m^3/s)/m^3.

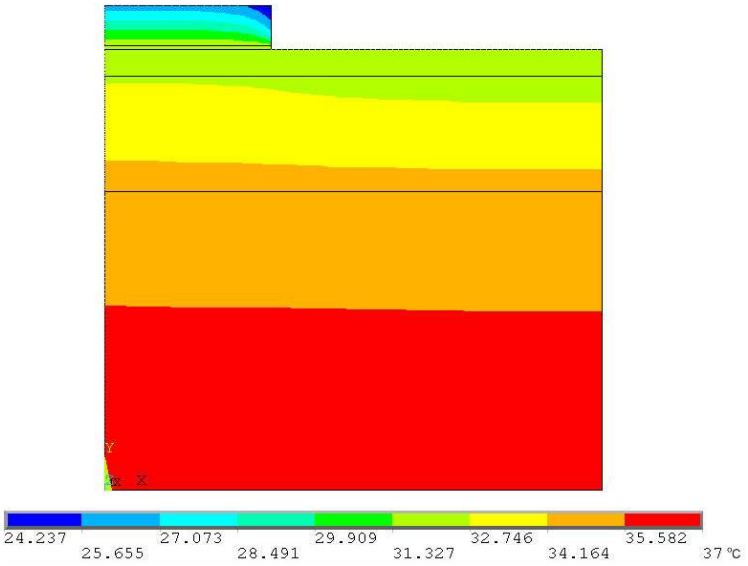

Fig. 2.18 Temperature contour diagram for k = 0.03 W/m-^{o}C and ω_b = 0 (m^3/s)/m^3.

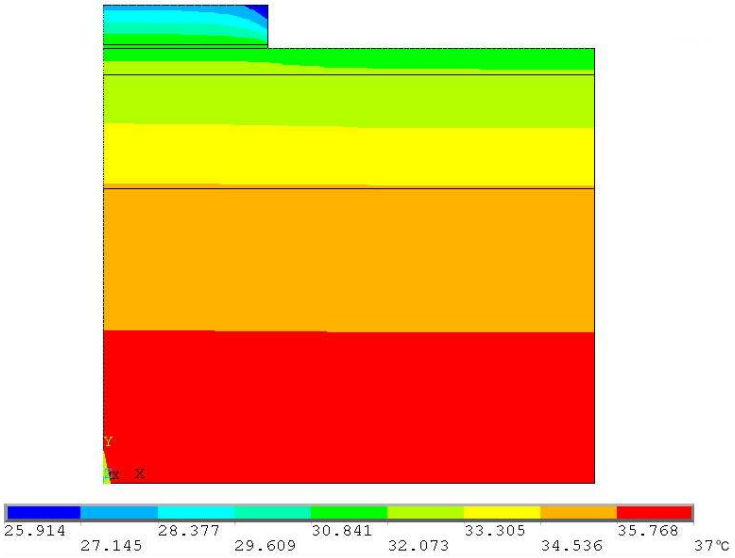

Fig. 2.19 Temperature contour diagram for k = 0.06 W/m-^{o}C and ω_b = 0 (m^3/s)/m^3.

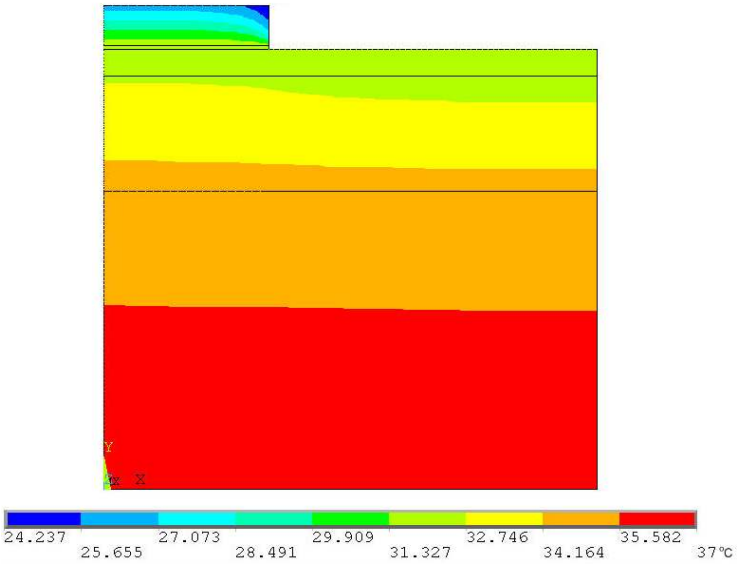

Fig. 2.20 Temperature contour diagram for k = 0.03 W/m-^{o}C and ω_b = 0.001 (m^3/s)/m^3.

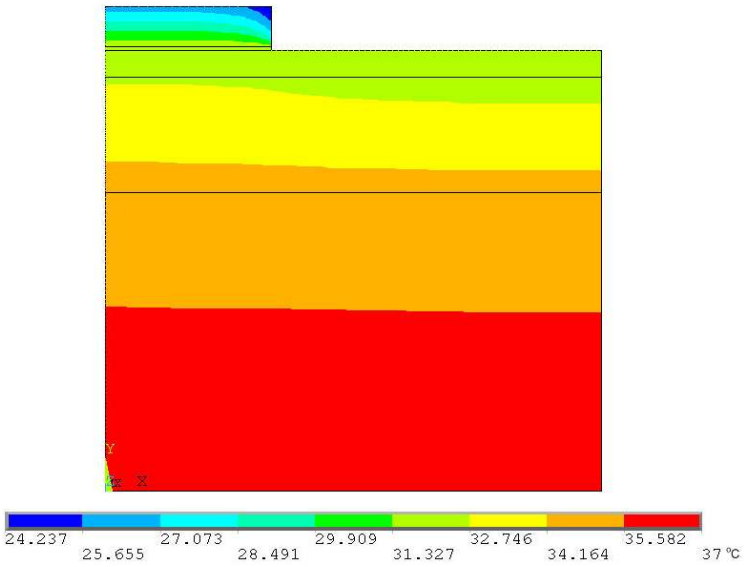

Fig. 2.21 Temperature contour diagram for k = 0.03 W/m-^{o}C and ω_b = 0.005 (m^3/s)/m^3.

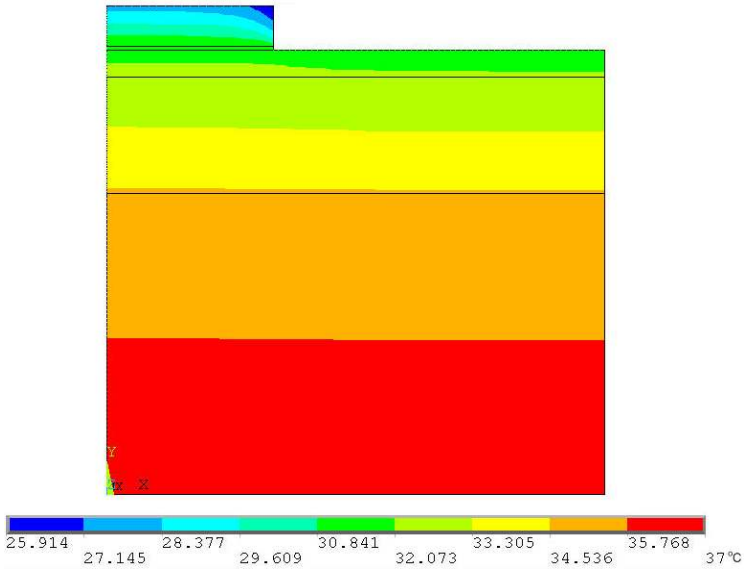

Fig. 2.22 Temperature contour diagram for k = 0.06 W/m-^{o}C and ω_b = 0.001 (m^3/s)/m^3.

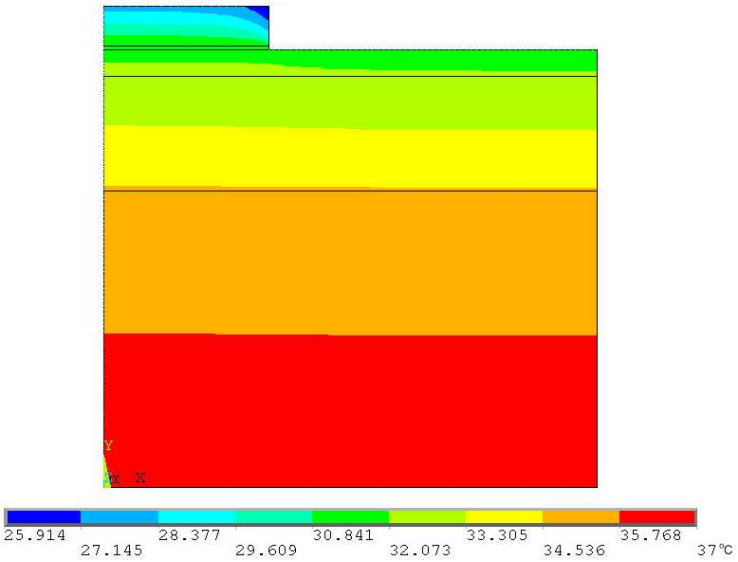

Fig. 2.23 Temperature contour diagram for k = 0.06 W/m-^{o}C and ω_b = 0.005 (m^3/s)/m^3.

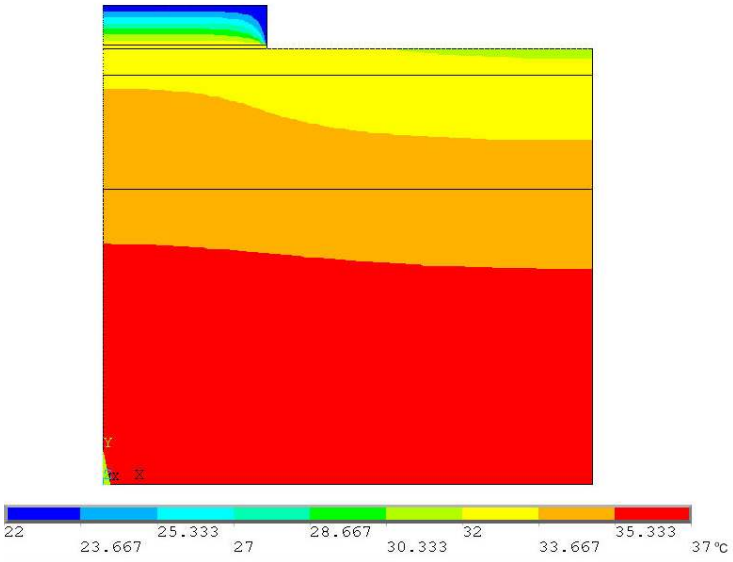

Fig. 2.24 Temperature contour diagram for k = 0 W/m-^{o}C and ω_b = 0.001 (m^3/s)/m^3.

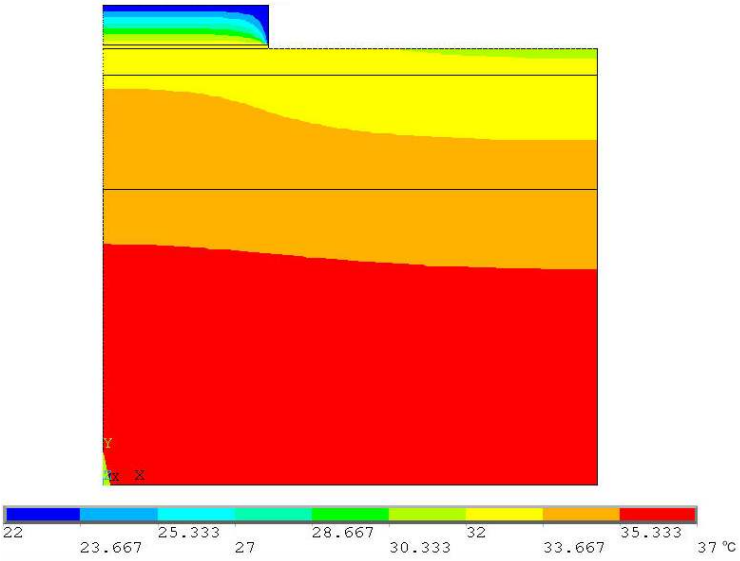

Fig. 2.25 Temperature contour diagram for k = 0 W/m-^{o}C and ω_b = 0.005 (m^3/s)/m^3.

In Figure 2.26, it is seen that with a finer mesh of 23,600 elements, the temperature contour diagram is sensibly the same as with a mesh of 11,800 elements. This result confirms the mesh-independence study previously discussed.

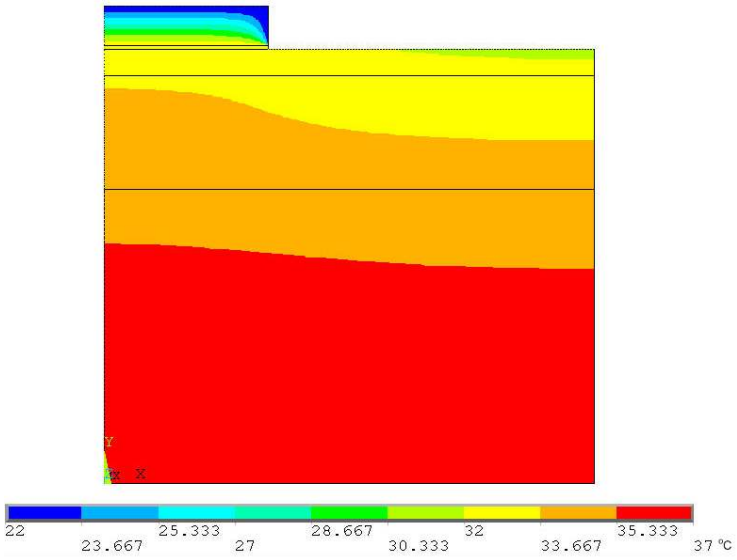

Fig. 2.26 Temperature contour diagram for k = 0 W/m-^{o}C and ω_b = 0.005 (m^3/s)/m^3 with 23,600 elements.

2.4.1 Heat Flux Diagrams

Figures 2.27, 2.28, and 2.29 display vector diagrams showing the paths of heat flow. The extreme case of $k = 0$ corresponds to the diagram for which the departures from an array of straight, vertical heat flow lines is the greatest. Inspection of the figure shows that the blockage of the heat flow is greatest near the outer edge of the temperature measurement device, as evidenced by the outward-directed vectoring. The presence of the thin, heat-spreading copper foil situated at the base of the device is made evident by the horizontal outward-directed vectors that lie in the plane of the foil. Aside from these features, most of the diagram shows upward-directed vectors.

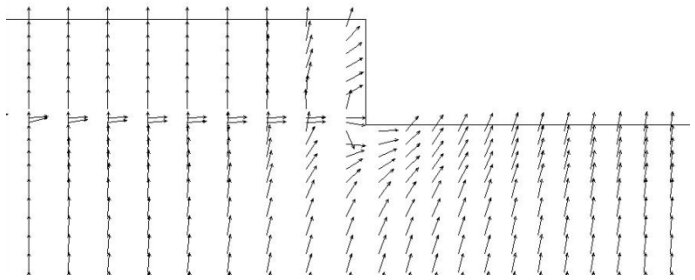

Fig. 2.27 Vector heat flux diagram for k = 0 W/m-^{o}C and ω_b = 0.003 (m^3/s)/m^3.

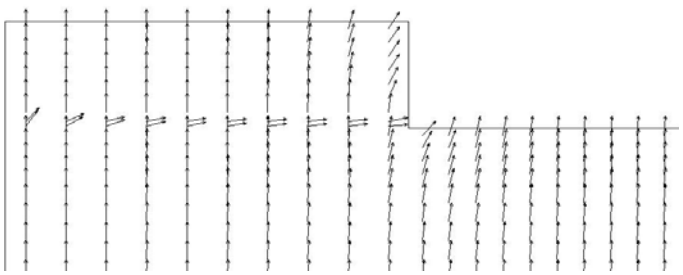

Fig. 2.28 Vector heat flux diagram for k = 0.03 W/m-^{o}C and ω_b = 0.003 (m^3/s)/m^3.

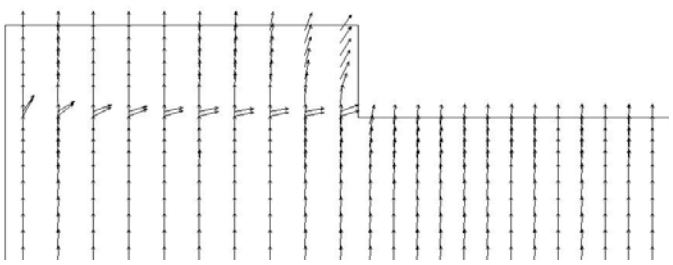

Fig. 2.29 Vector heat flux diagram for k = 0.06 W/m-^{o}C and ω_b = 0.003 (m^3/s)/m^3.

2.5 Concluding Remarks

In clinical practice, it is common to measure skin-surface temperature by making use of a direct-contact device which is affixed to the skin by means of an adhesive film. Physical intuition would argue that such a device should be constituted so that it does not obstruct the heat flow between the skin surface and the surroundings. It is, therefore, remarkable that common direct-contact, skin-surface temperature measurement devices incorporate a foam pad in their construction. The assessment of the measurement errors caused by the presence of such insulation pads has been the focus of this investigation. The magnitude of the thermal conductivity of the pad was found to be the controlling parameter with respect to the temperature measurement error. In the limiting case of a conductivity of zero, the calculated measurement error is 1.5 ^{o}C. For conductivities of 0.03 and 0.06 W/m-^{o}C, the calculated errors are 0.5 and 0.15 ^{o}C, respectively. The magnitude of the rate of blood perfusion was found to have an insignificant effect on the measured temperatures.

CHAPTER 3

TRANSIENT

3.1 Introduction

Up until now, only the steady state has been considered. However, in a clinical setting, the time to reach steady state is of practical importance. In the present chapter, transient numerical simulation of the temperature distribution and heat flow in human tissue beneath skin in the presence of a skin-surface measuring device is undertaken. The skin, fat, and muscle in the absence of the sensor will be assumed to have reached steady-state. At time $t = 0$, the sensor (which is initially at room temperature) will be placed onto the surface of the skin. The time to reach steady-state will be investigated. Again, the multi-dimensional transient bioheat equation is used as the analysis tool.

3.2 Physical Model

In the present problem, the same axisymmetric model used in Chapter 2 will be used to investigate the errors of skin-surface temperature measurements in transient conditions. This model is displayed in Fig. 3.1.

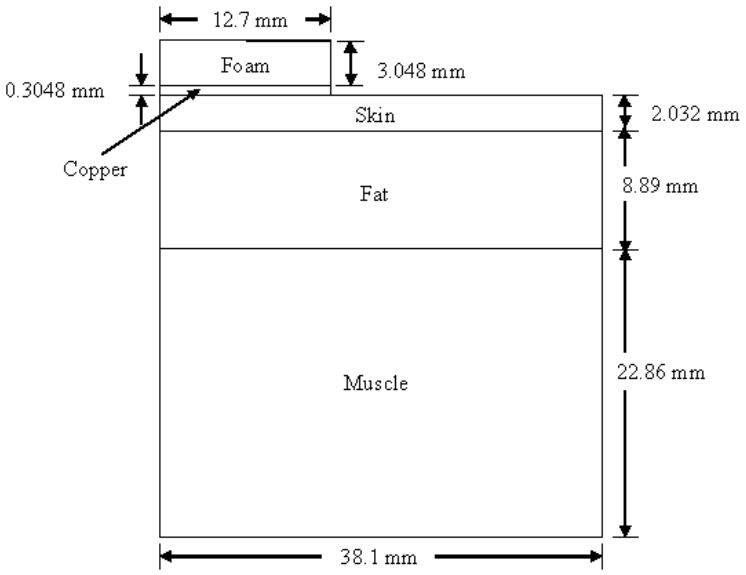

Fig. 3.1 Schematic diagram of an axisymmetric view of the foam and copper spreader placed onto a section of skin, fat, and muscle.

At the exposed surfaces of the skin and of the temperature measurement device, heat loss by convection to the ambient air and by radiation to surrounding solid objects is taken into account in the simulation. The lower surface of the muscle layer is taken to be at the body temperature (37 ^{o}C). The right-hand vertical boundary of the solution space, situated beyond the reach of the disturbance caused by the measuring device, is considered as adiabatic.

3.3 Analysis

An analysis of the error in the transient temperature measurement is performed. The Pennes bioheat equation is used to describe the heat transfer inside tissue. The axisymmetric form of the transient Pennes bioheat equation is as follows

$$\rho c \frac{\partial T}{\partial t} = k\left[\frac{1}{r}\frac{\partial}{\partial r}\left(r\frac{\partial T}{\partial r}\right) + \frac{\partial^2 T}{\partial z^2}\right] + \omega_b \rho_b c_b (T - T_c) \tag{3.1}$$

Equation (3.1) is applied separately in the skin, fat, and muscle layers. Therefore, the properties k, ρ and c pertain to the tissue in the respective layers. The density ρ_b and specific heat c_b pertain to blood and are the same for the body layers. The blood perfusion rate ω_b has units of m^3/s per m^3 of tissue. The temperature T corresponds to the local tissue temperature and T_c to the body core temperature. The metabolic heat generation is not included in Eq. (3.1) because it is negligible compared to the perfusion term.

Heat conduction in the measurement device is governed by the following equation

$$\rho c \frac{\partial T}{\partial t} = k\left[\frac{1}{r}\frac{\partial}{\partial r}\left(r\frac{\partial T}{\partial r}\right) + \frac{\partial^2 T}{\partial z^2}\right] \tag{3.2}$$

The properties ρ, c and k pertain respectively to the foam pad and the copper heat spreader.

The initial temperature of the sensor and foam is the ambient temperature taken to be equal to 22°C. The initial condition of the skin, fat and muscle is taken to be the steady-state temperature distribution of the respective layers in the absence of the sensor. Therefore, a steady-state simulation without the temperature-measuring device is first solved. Then, the corresponding solution of the steady state problem without the device

is used as initial input for the body layers into the time-dependent solution. At time t = 0, the sensor is stuck onto the surface of the skin.

At the exposed surfaces to the environment of the skin and the temperature measurement device,

$$-k\left(\frac{\partial T}{\partial n}\right) = h(T - T_{\infty}) \tag{3.3}$$

The conductivity is that of the skin, the foam, or the copper, h is the combined convective and radiative heat transfer coefficients, and T_{∞} is the temperature of the ambient air and the surrounding solid objects. The following values are used, h = 13.63 W/m^2-^{o}C and T_{∞} = 22 ^{o}C. Figure 3.2 illustrates the boundary conditions for the transient problem.

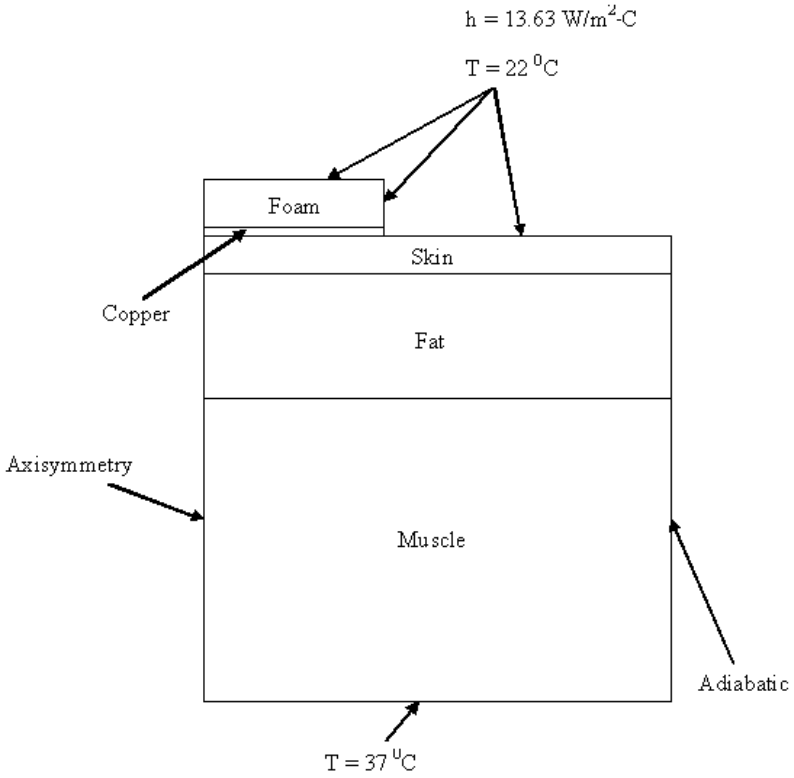

Fig. 3.2 Boundary conditions for the transient problem.

Continuity of temperature and heat flux is required at the interfaces of the layers. As already noted, the outboard lateral surface of the solution space is adiabatic, and the temperature of the bottom of the muscle layer is at 37 ^{o}C. Also, T_c in Eq. (3.1) is taken to be 37 ^{o}C.

At time t = 0, the initial temperature of the skin, fat, and muscle will be the steady-state temperature of the tissue without the sensor present. The steady solution will first be simulated, and the results be used as input for the initial conditions of the skin, fat, and muscle in the transient simulation. The boundary conditions used to obtain the steady state solution for an initial condition to the transient analysis are illustrated in Fig. 3.3.

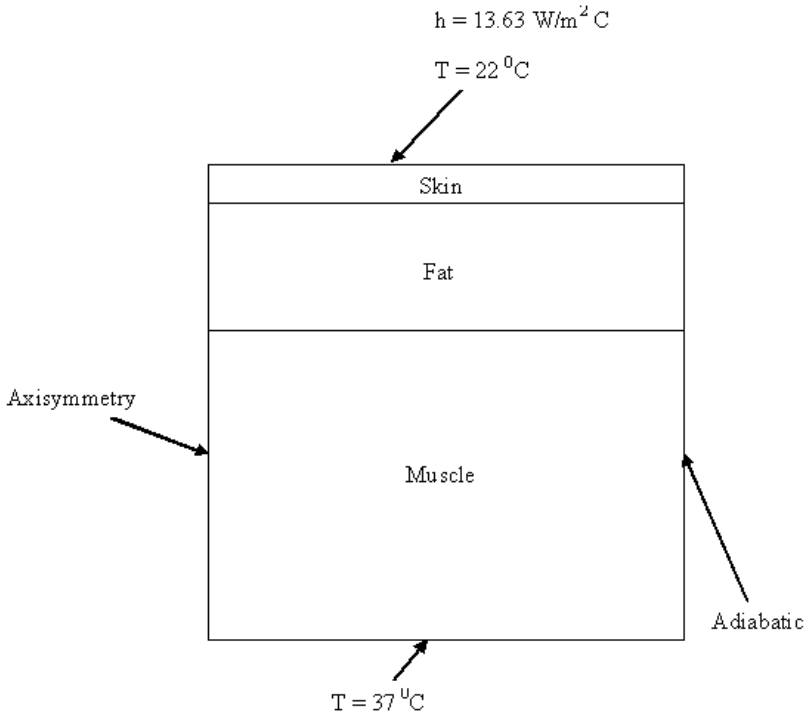

Fig. 3.3 Boundary conditions for the steady problem.

The initial temperature of the sensor will be that of the ambient air (22 ^{o}C).

Table 3.1 lists the thermophysical properties of the materials. Since the study is transient, the values of the density and the specific heat of the materials need to be included. In Chapter 1, it was determined that the value of the perfusion had a minor effect impact on the solution, therefore the intermediary value of $\omega_b = 0.003$ $(m^3/s)/m^3$ is chosen. The thermal conductivities of the foam for the skin, fat and muscle layers are varied parametrically.

Table 3.1 Material properties used in the transient simulation.

	k [W/m-^{o}C]	ρ [kg/m^3]	c [J/kg-^{o}C]	$\rho_b c_b$ [J/m^3-^{o}C]	ω_b [(m^3/s)/m^3]
Skin	0.62	1100	3500		
Fat	0.48	960	2500	4×10^6	0.003
Muscle	1.26	1040	3600		
Foam	0, 0.03, 0.06	24	1130		
Copper	380.51	8933	385		

The numerical simulations are performed using ANSYS 11.0 finite-element software. The number of nodes used in the execution of the solution is the same number as for the steady-state study, namely 118,000 nodes. The time step size used is 0.1 s.

3.4 Results and Discussion

The temperature contour diagram of the steady-state solution in the absence of the skin-temperature measurement device is shown in Fig. 3.4. As seen in the figure, the isotherms are straight and horizontal (one-dimensional).

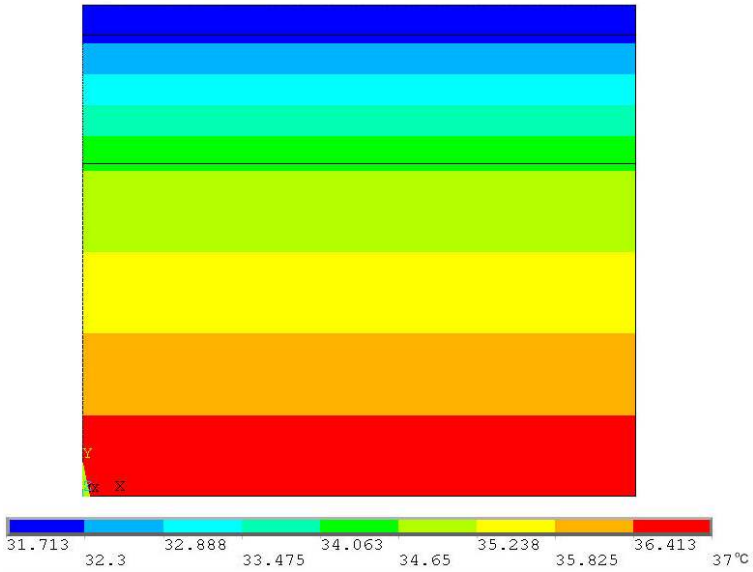

Fig. 3.4 Temperature contour diagram of the steady-state solution in the absence of the skin-surface temperature measuring device.

The duration for which it takes to reach steady state is determined for the three values of the thermal conductivity. In Fig.3.5, the temperature versus time at two points at the interface between the skin and the temperature measurement device is plotted. The two points chosen were the center of the skin-temperature measuring device and the edge of the measuring device. It is seen that the less the thermal conductivity of the foam is, the longer it takes for the temperature to reach steady state. For the insulated case, which

corresponds to a value of thermal conductivity equal to zero, it takes about 4,900 seconds to reach steady state. That is approximately one hour and twenty-one minutes. However, for the other values of thermal conductivity of the foam, equal to 0.03 and 0.06, it takes only 3,000 seconds or 50 minutes for the temperature to reach steady state.

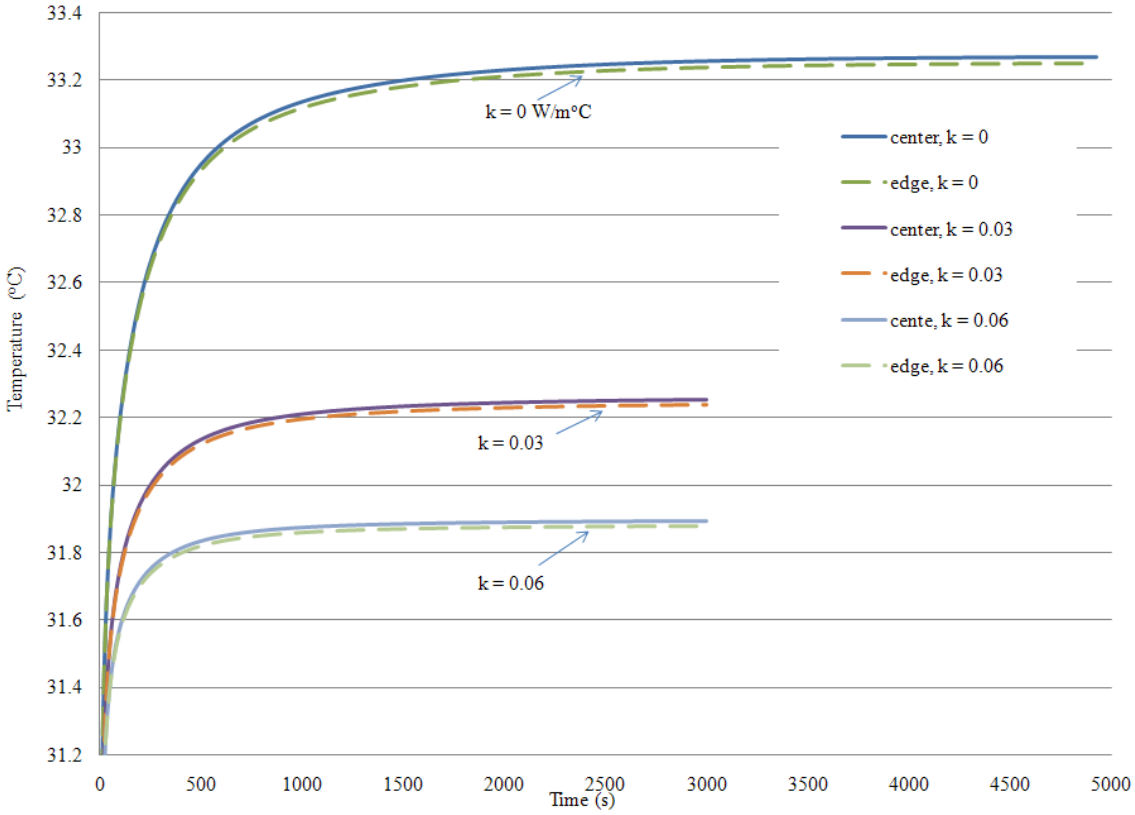

Fig. 3.5 Temperature of the interface of the device and the skin surface at two different locations versus time for the three values of the foam thermal conductivity.

In Fig. 3.6, the temperature of two different locations at the interface of the device and the skin surface is plotted versus time for a foam pad conductivity of k = 0.03 W/m-^{o}C. It is seen there that the duration of the transient period, the temperature at the

interface of the heat spreader and skin doesn't depend on the radial position. Indeed, as shown in Figure 3.6, the temperature evolution at the two different locations is the same. There is little variation of the temperature underneath the pad.

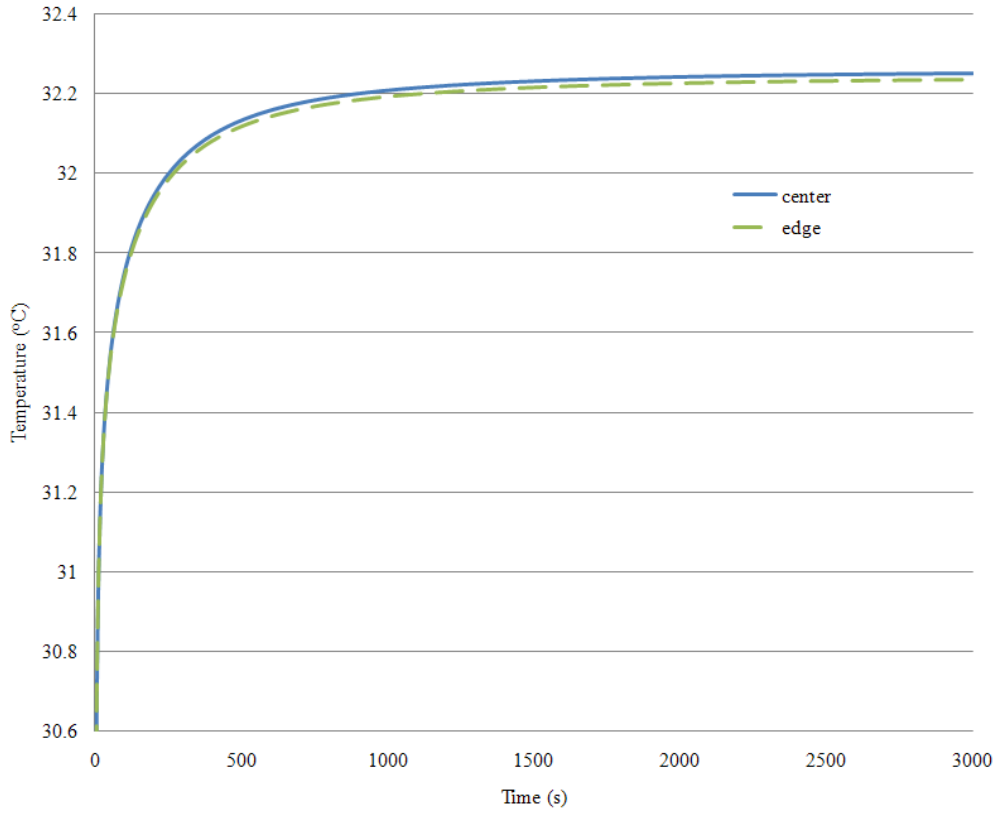

Fig. 3.6 Temperature of the interface of the device and the skin surface at at two different locations versus time for k = 0.03 W/m-^{o}C.

Temperature contour diagrams are presented in Figures 3.7, 3.8 and 3.9, respectively at 0.1 s, 50 s and 4,926 s for the case k = 0 W/m-^{o}C.

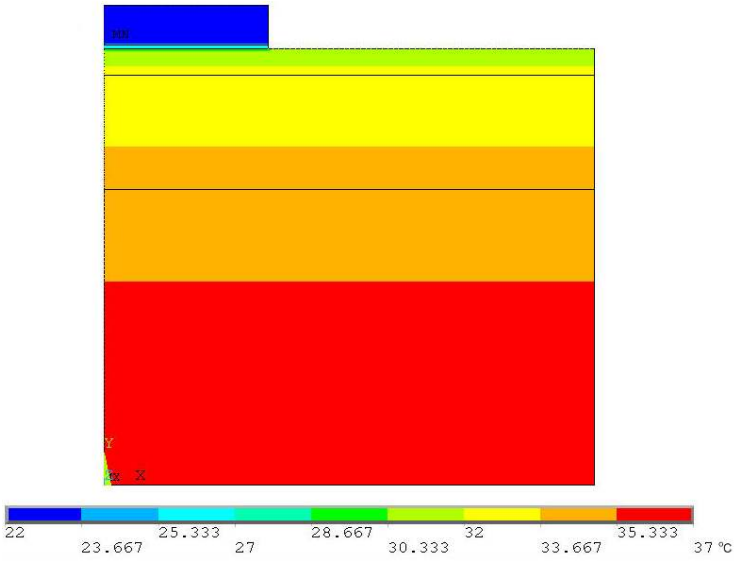

Fig. 3.7 Temperature contour diagram for k = 0 W/m-^{o}C at 0.1 s.

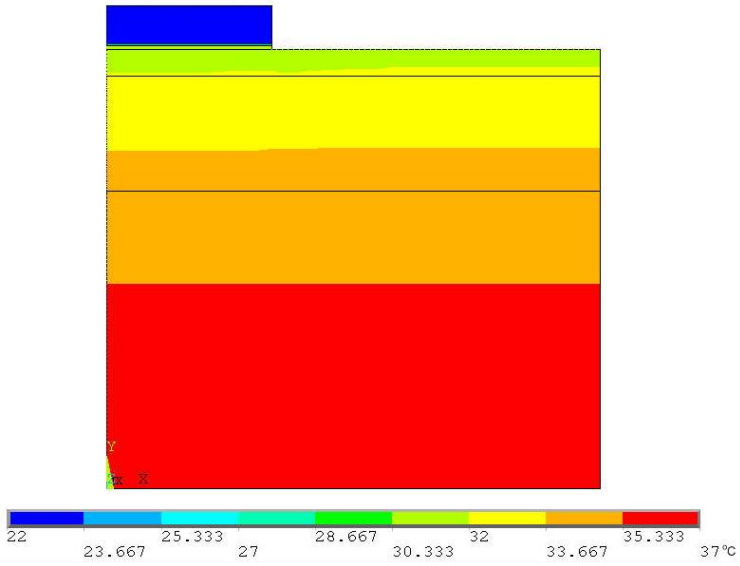

Fig. 3.8 Temperature contour diagram for k = 0 W/m-^{o}C at 50 s.

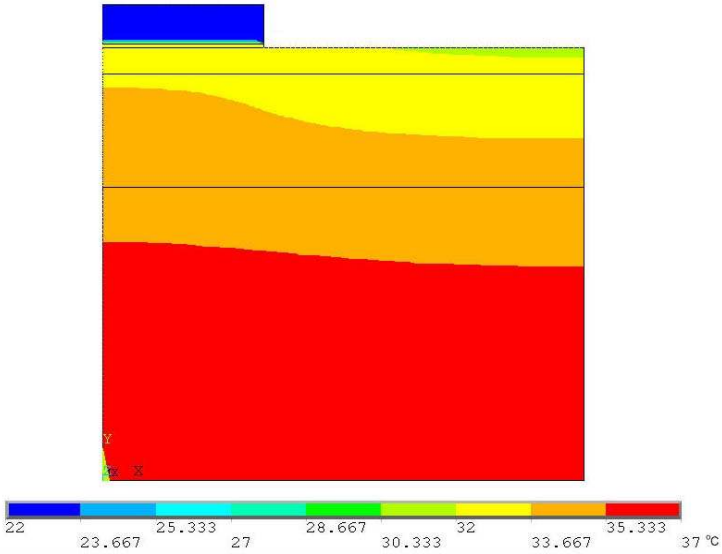

Fig. 3.9 Temperature contour diagram for k = 0 W/m-^{o}C at 4,926 s.

Temperature contour diagrams are presented in Figs. 3.10, 3.11 and 3.12, respectively at 0.01 s, 50 s and 3,000 s for the case k = 0.03 W/m-^{o}C. It takes about 3,000 s for the temperature to reach steady state as shown in Fig. 3.12.

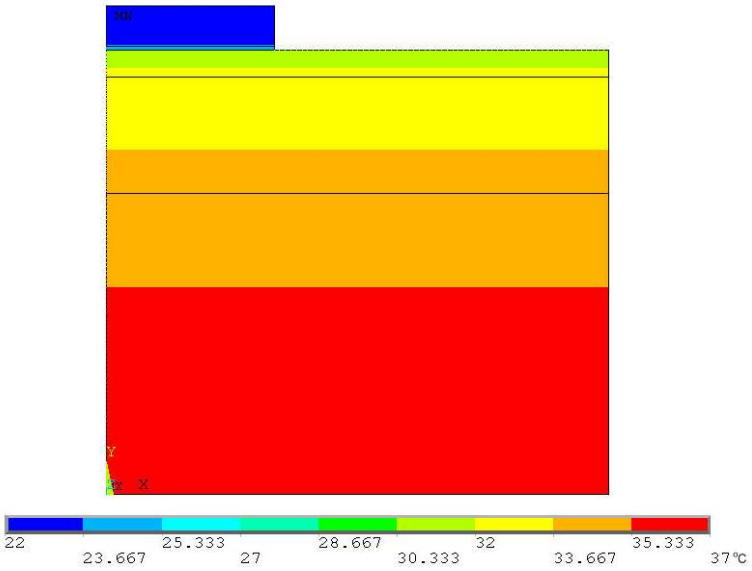

Fig. 3.10 Temperature contour diagram for k = 0.03 W/m-^{o}C at 0.01 s.

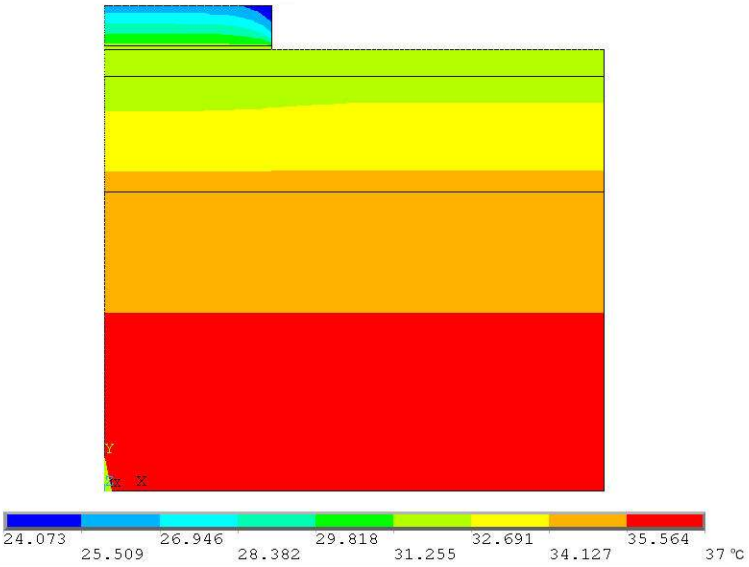

Fig. 3.11 Temperature contour diagram for k = 0.03 W/m-^{o}C at 50 s.

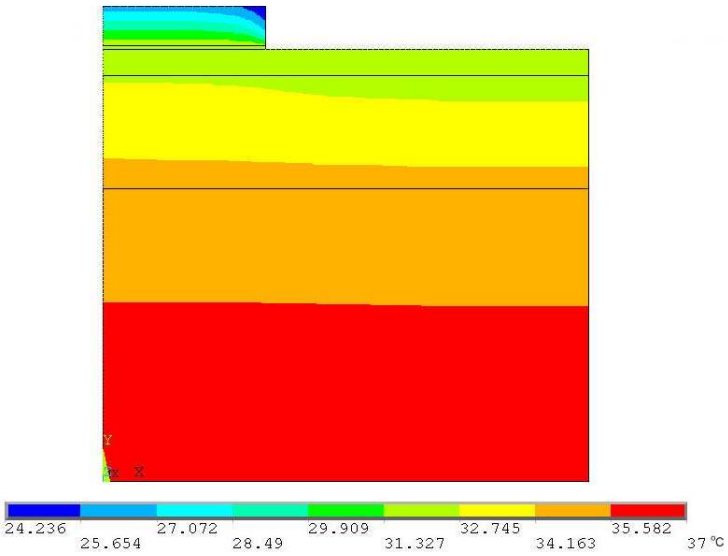

Fig. 3.12 Temperature contour diagram for k = 0.03 W/m-^{o}C at 3,000 s.

Temperature contour diagrams are presented in Figs. 3.13, 3.14 and 3.15, respectively at 0.1 s, 50 s and 3,000 s for the case k = 0 W/m-^{o}C. As shown in Fig. 3.15, it takes about 3,000 s for the temperature to reach steady state.

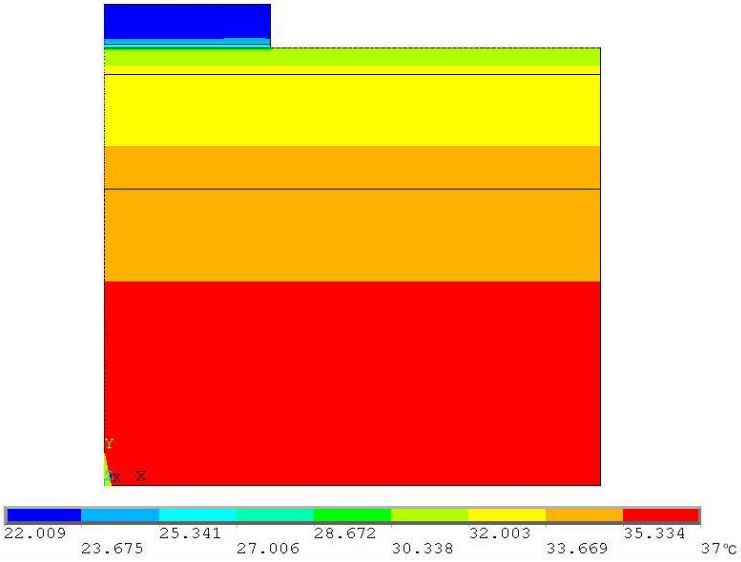

Fig. 3.13 Temperature contour diagram for k = 0.06 W/m-^{o}C at 0.1 s.

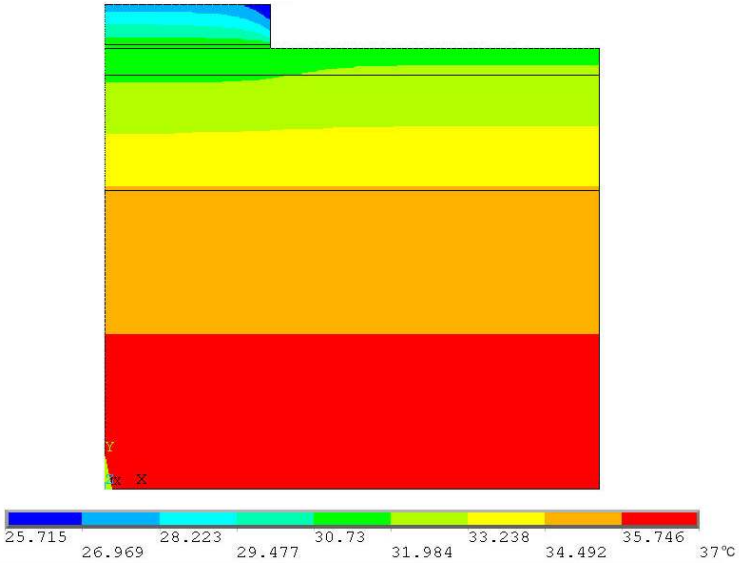

Fig. 3.14 Temperature contour diagram for k = 0.06 W/m-^{o}C at 50 s.

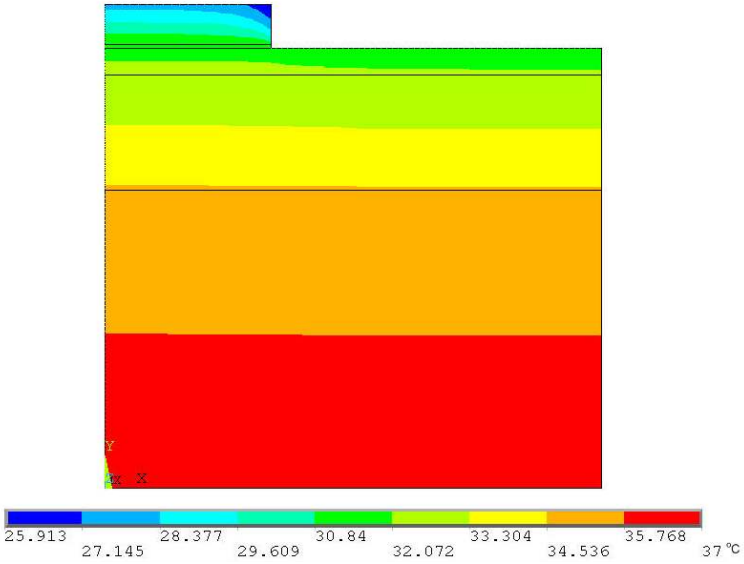

Fig. 3.15 Temperature contour diagram for k = 0.06 W/m-^{o}C at 3,000 s.

3.5 Concluding Remarks

The determination of the time it takes to reach steady state for the temperature and the variation of the temperature underneath the instrumentation device has been the focus of this investigation. The magnitude of the thermal conductivity of the pad was found to be the controlling parameter with respect to the transient time. In the limiting case of a conductivity of zero, the calculated time is about 4,900 s. For conductivities of 0.03 and 0.06 W/m-^{o}C, the calculated time is 3,000 s. Even though the time to reach steady state is less for the more realistic values of k = 0.03 W/m-^{o}C and 0.06 W/m-^{o}C, the actual times are unacceptable in a clinical study. Therefore, like in standard digital thermometers, a curve fit and extrapolation formula is needed to be in order to determine the steady-state temperature from a shorter data collection period.

CHAPTER 4

INVESTIGATION OF THE FOAM PAD

4.1 Introduction

As was concluded in Chapter 1, the foam insulating pad presents a problem in obtaining accurate skin-surface temperature results. In order to alleviate the problem, several simulations will be performed. The effect of reducing the foam-pad thickness in half as well as completely removing the pad will be investigated. In this Chapter, all boundary conditions, initial conditions, material properties and geometries not directly specified here will remain as in Chapters 1 and 2. Again, the value taken for the blood perfusion will be $\omega_b = 0.003$ $(m^3/s)/m^3$. All solutions will be run as time-dependent.

4.2 Reduction of the Foam Pad Thickness by Half

The thickness of the foam pad is reduced by half to 1.524 mm thick and the assembly will be numerically simulated. Figure 4.1 displays the temperature versus time of two locations at the interface of the skin and the sensor. Figures 4.2 displays the temperature contour diagram of the system for a thermal conductivity of the foam pad equal to $k = 0$ W/m-^oC.

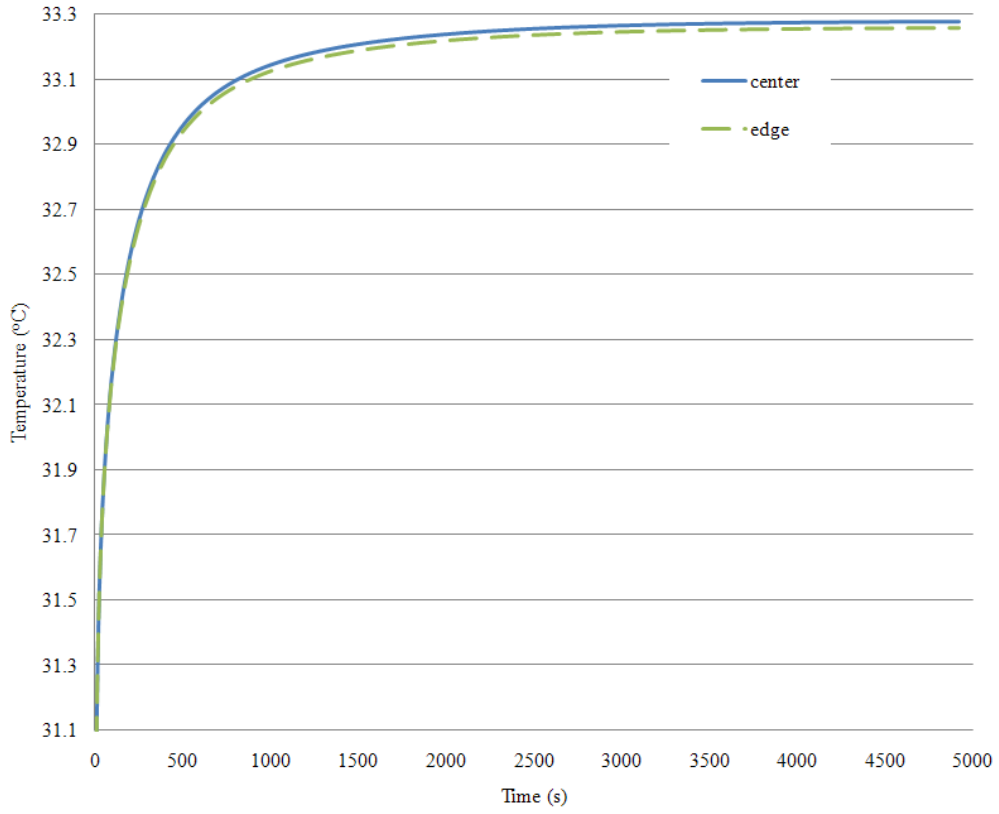

Fig. 4.1 Temperature of the interface of the device and the skin surface at two different locations underneath the copper heat spreader nodes versus time for k = 0 W/m-^{o}C.

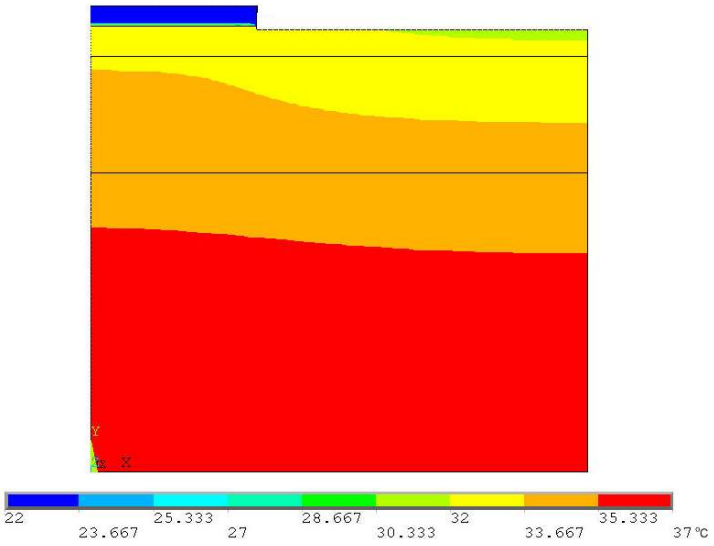

Fig. 4.2 Temperature contour diagram for k=0 W/m-^{o}C at 4,926 s.

Figures 4.3 and 4.4 respectively display the skin temperature at the interface skin-device at at two different locations and the temperature contour of the system for a thermal conductivity of the foam pad equal to k = 0.03 W/m-^{o}C. The figures show that the time to reach steady state is approximately 5,000 s which is essentially the same for the case for the full thickness of the foam pad.

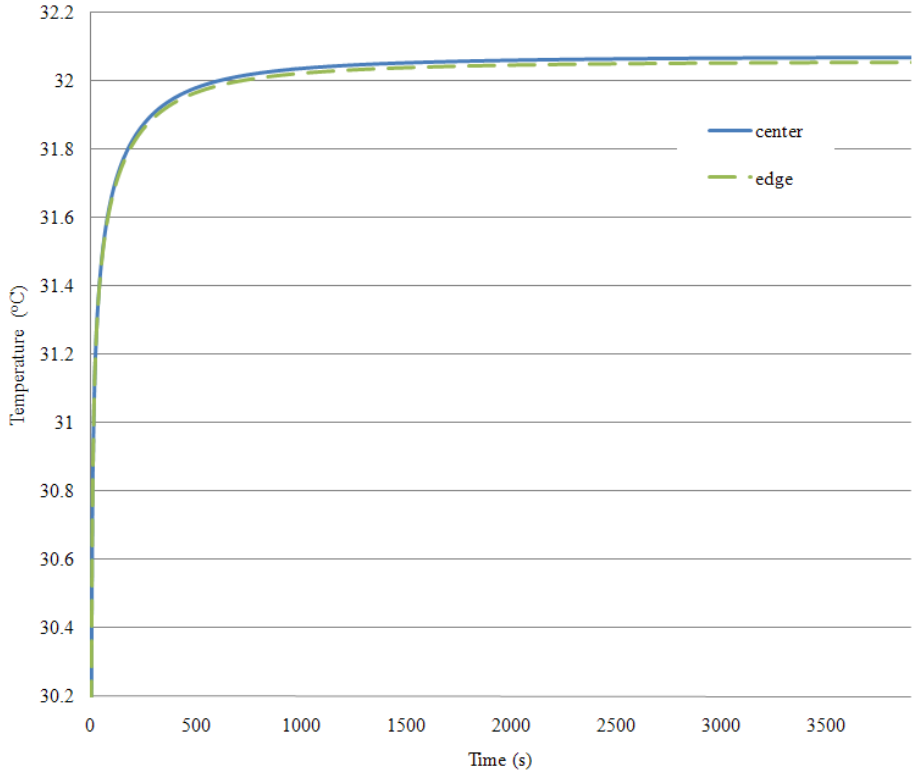

Fig. 4.3 Temperature of the interface of the device and the skin surface at two different locations underneath the sensor versus time for k = 0.03 W/m-°C.

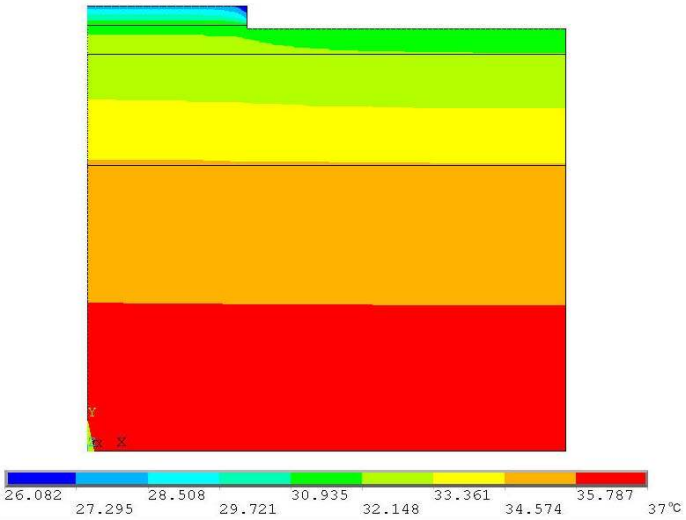

Fig. 4.4 Temperature contour diagram for k=0.03 W/m-°C at 3,942 s.

Figures 4.5 and 4.6 respectively display the skin temperature at the interface skin-device at at two different locations and the temperature contour of the system for a thermal conductivity of the foam pad equal to k = 0.06 W/m-^{o}C.

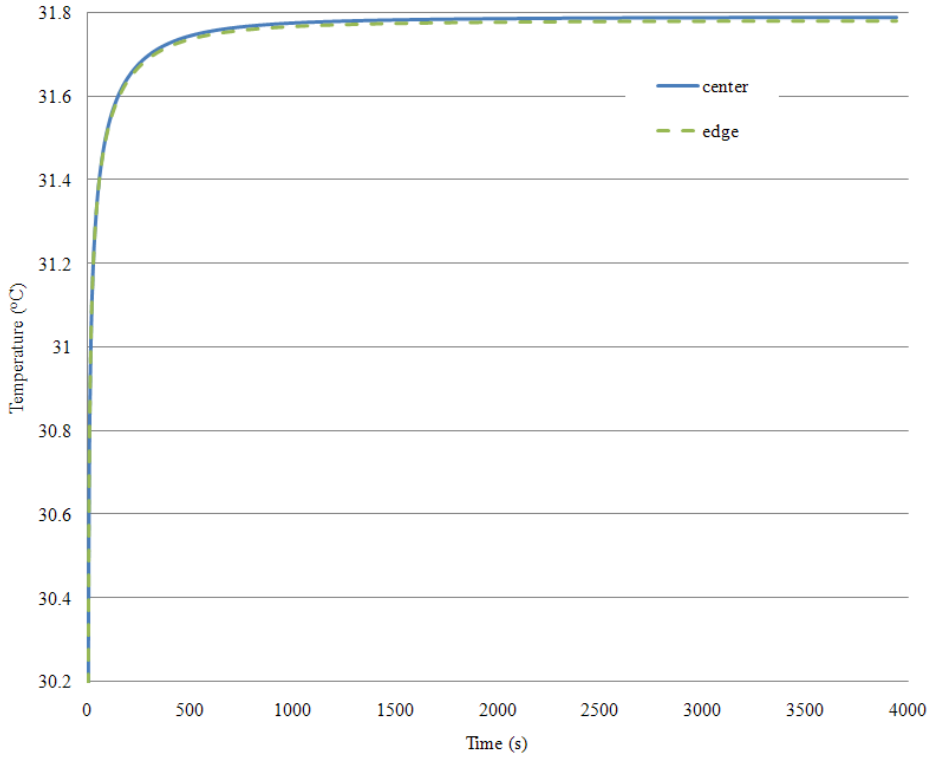

Fig. 4.5 Temperature of the interface of the device and the skin surface at two different locations underneath the sensor versus time for k = 0.06 W/m-^{o}C.

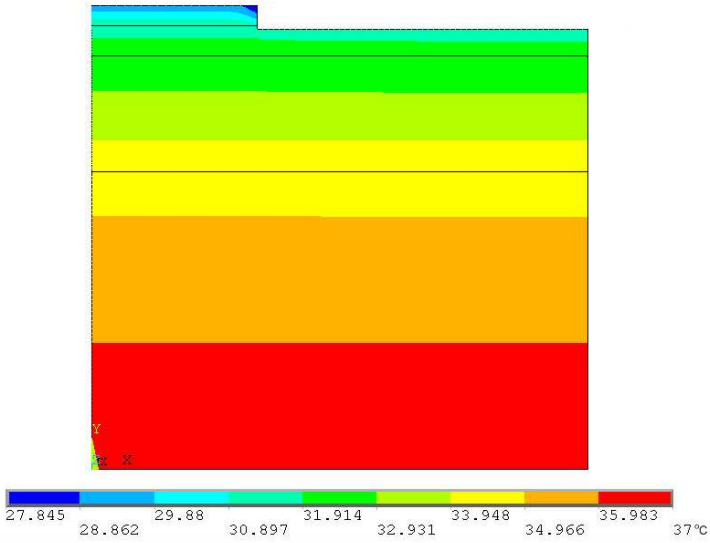

Fig. 4.6 Temperature contour diagram for k=0.06 W/m-^{o}C at 3,942 s.

In Figs 4.1, 4.3 and 4.5, it is shown that the temperature of the skin surface under the sensor decreases when the thickness of the foam pad is reduced. The error in temperature measurement is therefore less with a thinner foam pad.

4.2 Transient Study of the Temperature in the Absence of the Foam Pad

In this section, the foam pad is removed. The purpose of this study is to emphasize the role of the foam pad. Figures 4.7 and 4.8 respectively display the skin temperature at the interface of the skin and device skin-device at two different locations (center and edge) and the temperature contour of the system for the case without the foam pad.

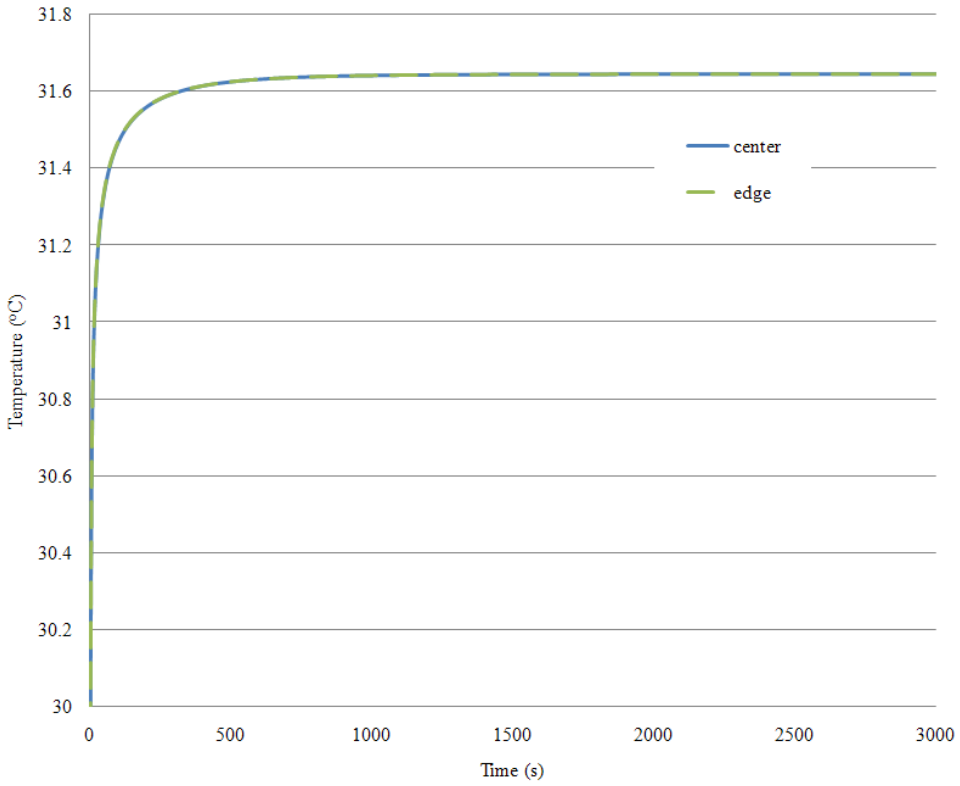

Fig. 4.7 Temperature of the interface of the device and the skin surface at two locations underneath the sensor versus time without the foam pad.

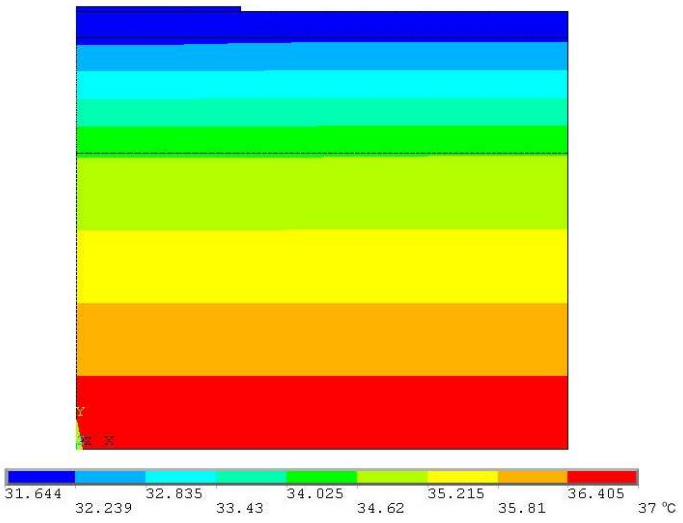

Fig.4.8 Temperature contour diagram at 4,920 s for the case without the foam pad.

In Fig. 4.8, it is noticed that the distribution of the temperature after about 4,900 s is similar to the temperature field at the initial condition. In addition, the thermal contour lines are straight and parallel, indicating minimum error in the skin-surface temperature measurement. The heat spreader, which is made of copper, acts as a thermal conductor from the surface of the skin to the environment.

Figures 4.9, 4.10, and 4.11 display the temperature transients for the two locations underneath the sensor for all values of thermal conductivity. As can be seen from the figures, it is advantageous to remove the foam pad altogether.

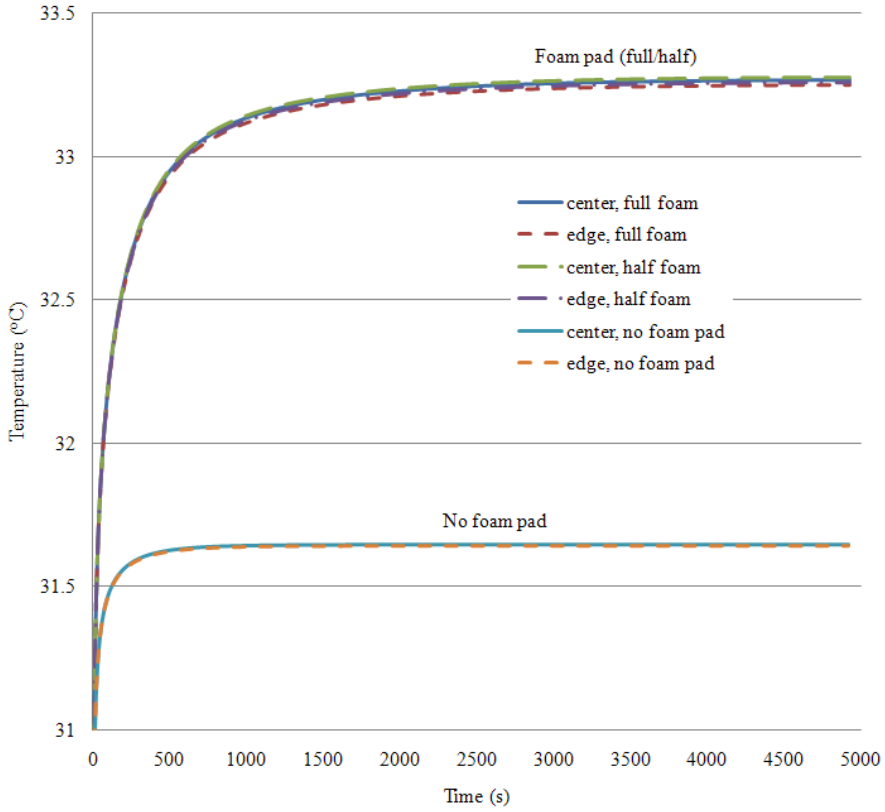

Fig. 4.9 Comparison of the temperature transients for the full foam pad, half foam pad, and no foam pad for k = 0 W/m-^{o}C.

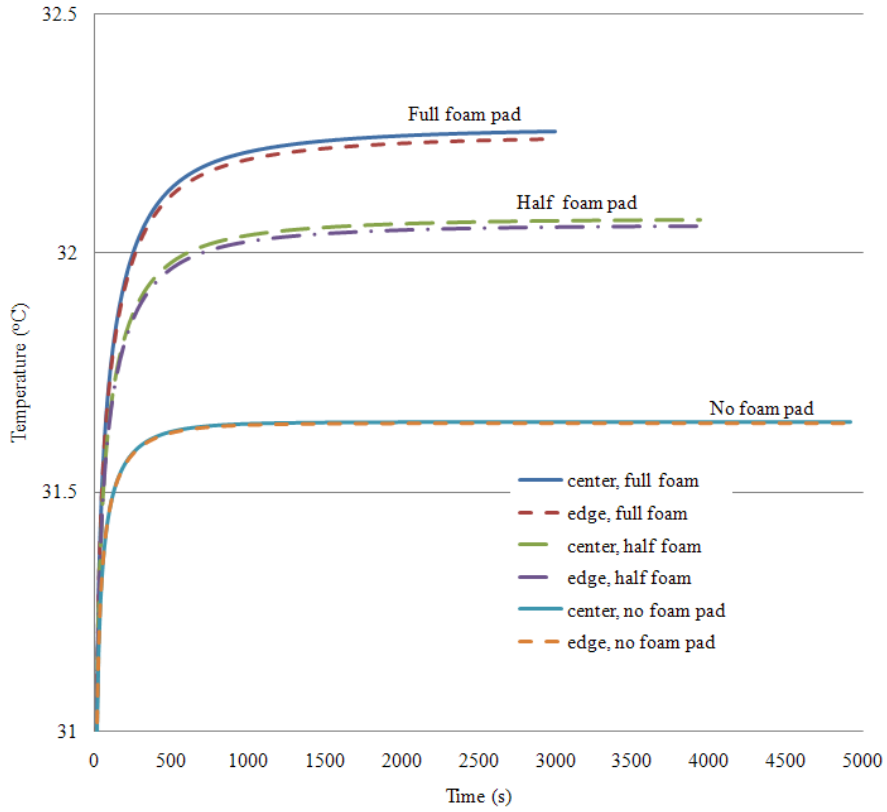

Fig. 4.10 Comparison of the temperature transients for the full foam pad, half foam pad, and no foam pad for k = 0.03 W/m-^{o}C.

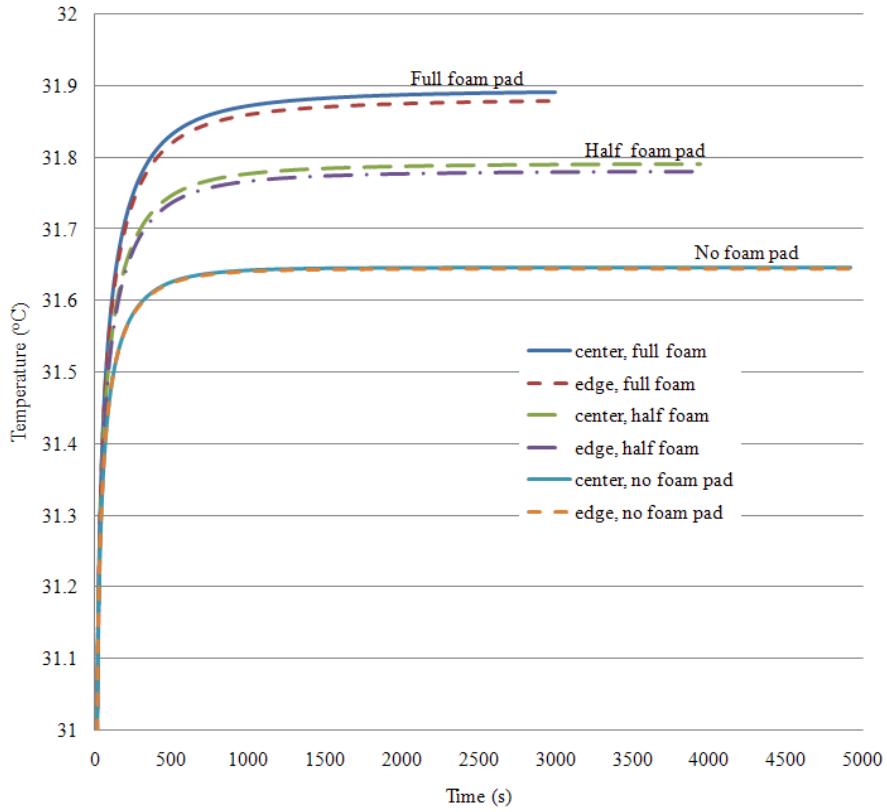

Fig. 4.11 Comparison of the temperature transients for the full foam pad, half foam pad, and no foam pad for k = 0.06 W/m-^{o}C.

CHAPTER 5

CONTACT RESISTANCE

5.1 Introduction of Air Gap to Model Contact Resistance

In the previous work described in this thesis, perfect thermal contact between the skin-surface temperature measuring device and the skin has been assumed. In reality, however, perfect thermal contact is usually not the case. Therefore, contact resistance must be taken into account. The contact resistance will be modeled as an air gap that is roughly the thickness of a sheet of paper. The air gap of 0.076 mm long is introduced between the skin surface and the measurement device to simulate the case when the sensor is not exactly in contact with the skin. In this section, only the full thickness of the foam pad and the removal of the foam pad altogether will be considered. The properties for the air used in the simulation are shown in Table 4.1.

Table 4.1 Material properties of the Air.

	k [W/m-^{o}C]	ρ [kg/m^{3}]	c [J/kg-^{o}C]
Air	0.0223	1.16	1007

5.2 Case with the Foam Pad

A first study of the presence of an air gap is undertaken with the foam pad. The thermal conductivity of the foam is chosen to be k = 0.03 W/m-^{o}C. Figures 5.1 and 5.2 respectively display the skin temperature at the interface skin-device at two different locations (center and edge) at the interface between the sensor and the skin surface. Also shown is the temperature contour of the system at steady state.

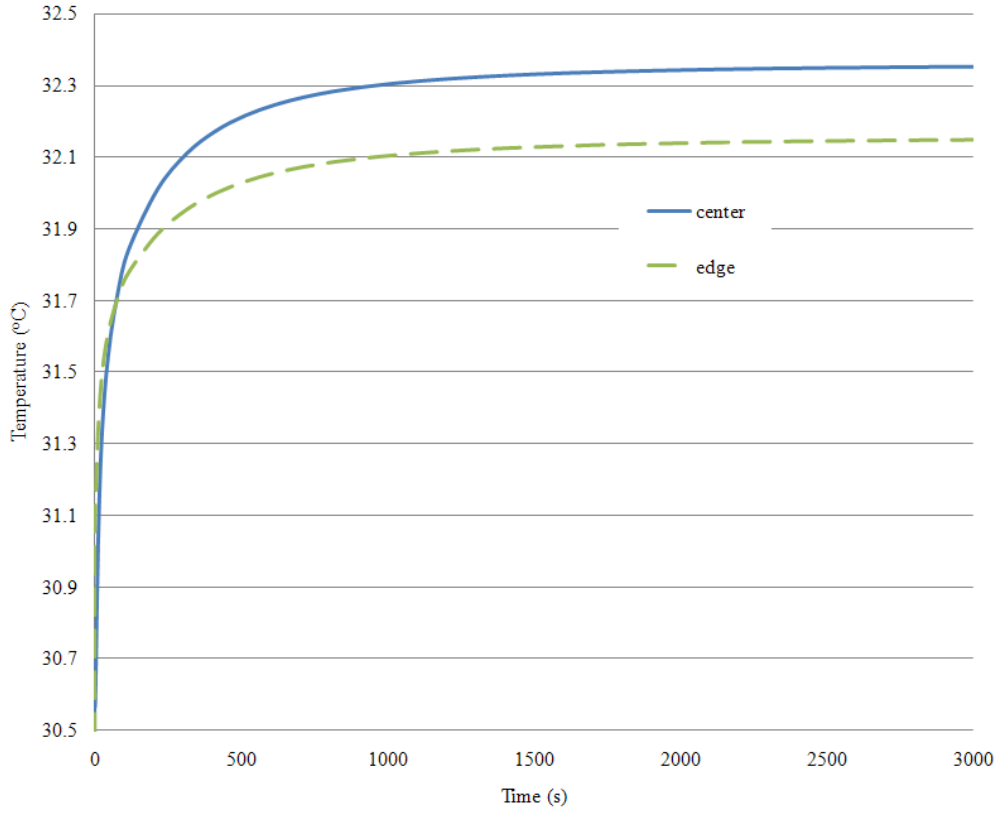

Fig.5.1 Temperature of the interface of the device and the skin surface at two different locations versus time for k = 0.03 W/m-^{o}C in the presence of an air gap.

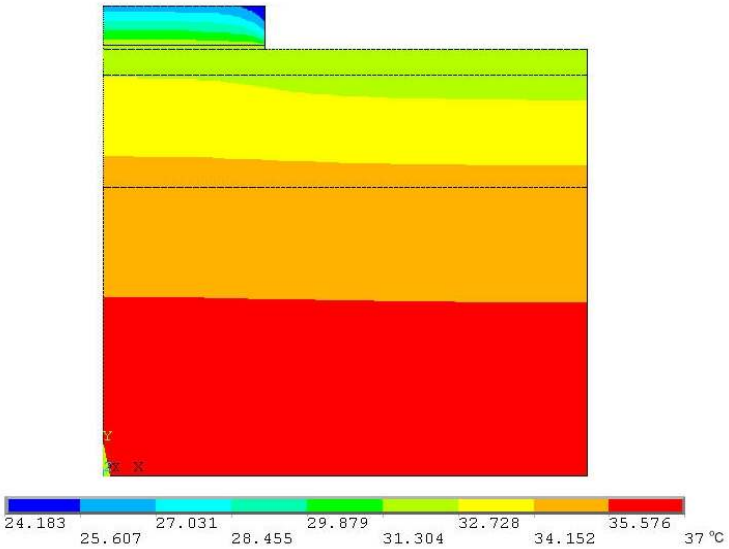

Fig. 5.2 Temperature contour diagram for k = 0.03 W/m-^{o}C at 10,000 s in the presence of an air gap.

A comparison of the case with air gap and the case without air gap in the presence of the foam pad is displayed in Fig. 5.3. According to the graph, not modeling the air gap produces an error of about 0.1 ^{o}C. Also, it is seen that the temperature distribution underneath the sensor is less uniform when an air gap is considered.

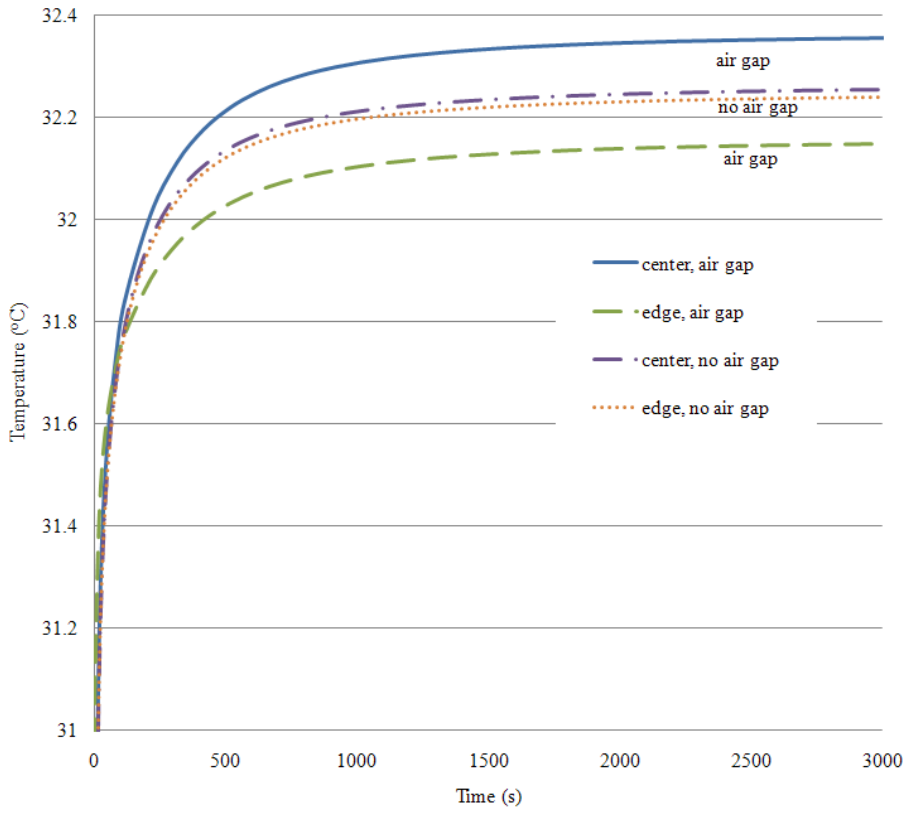

Fig. 5.3 Comparison of temperature transients with an air gap and for the case without an air gap and a foam thermal conductivity of k = 0.03 W/m-^{o}C.

5.3 Case Without the Foam Pad

A second study of the presence of an air gap is undertaken without the foam pad. Figures 5.4 and 5.5 respectively display the skin temperature at the interface skin-device underneath the sensor and the temperature contour diagram of the system.

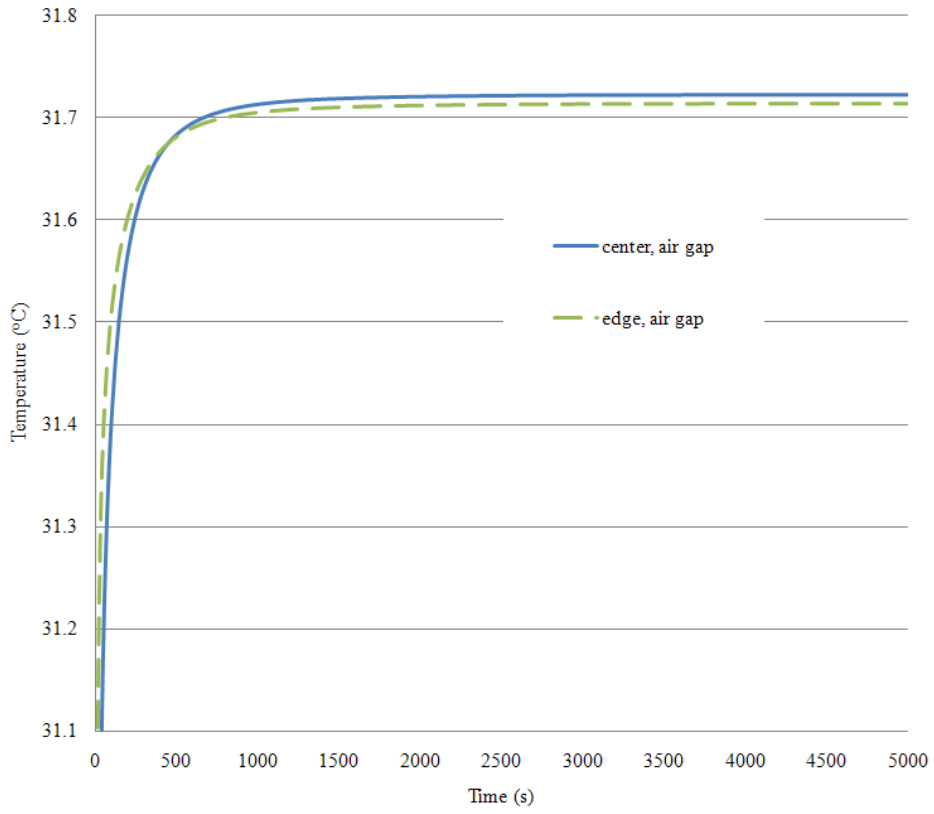

Fig. 5.4 Comparison of temperature transients in the presence of the air gap and without the foam pad.

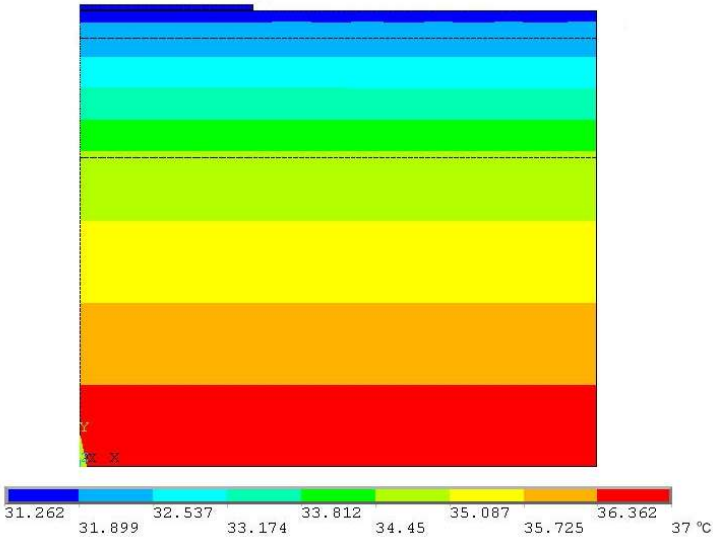

Fig. 5.5 Temperature contour diagram at 5,000 s in the presence of an air gap and without the foam pad.

A comparison of the case with the air gap and the case without air gap and without the foam pad is displayed in Fig. 5.6. It is shown that the presence of an air gap results in an increase of temperature of the skin surface under the temperature sensor device.

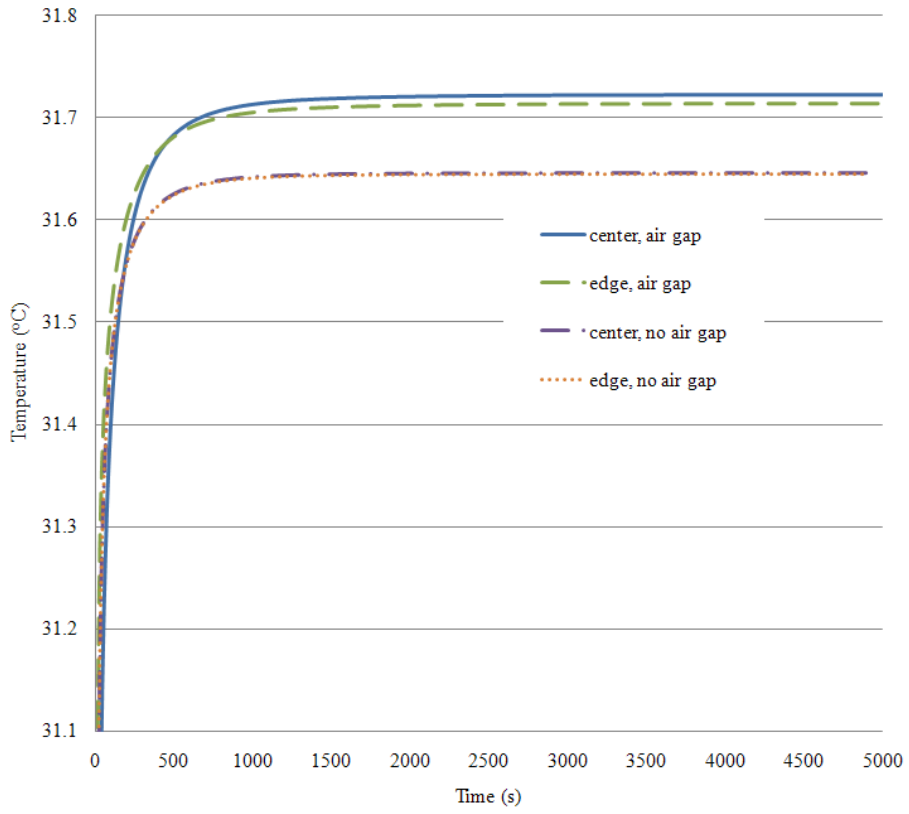

Fig. 5.6 Comparison of temperature variations for the case of measurement with an air gap and the case without air gap and without the foam pad.

Figure 5.7 is an all-encompassing graph of the temperature transients for the two locations underneath the sensor for foam, no foam, air gap, and no air gap. Here, the sensor reaches steady-state much quicker than for the foam.

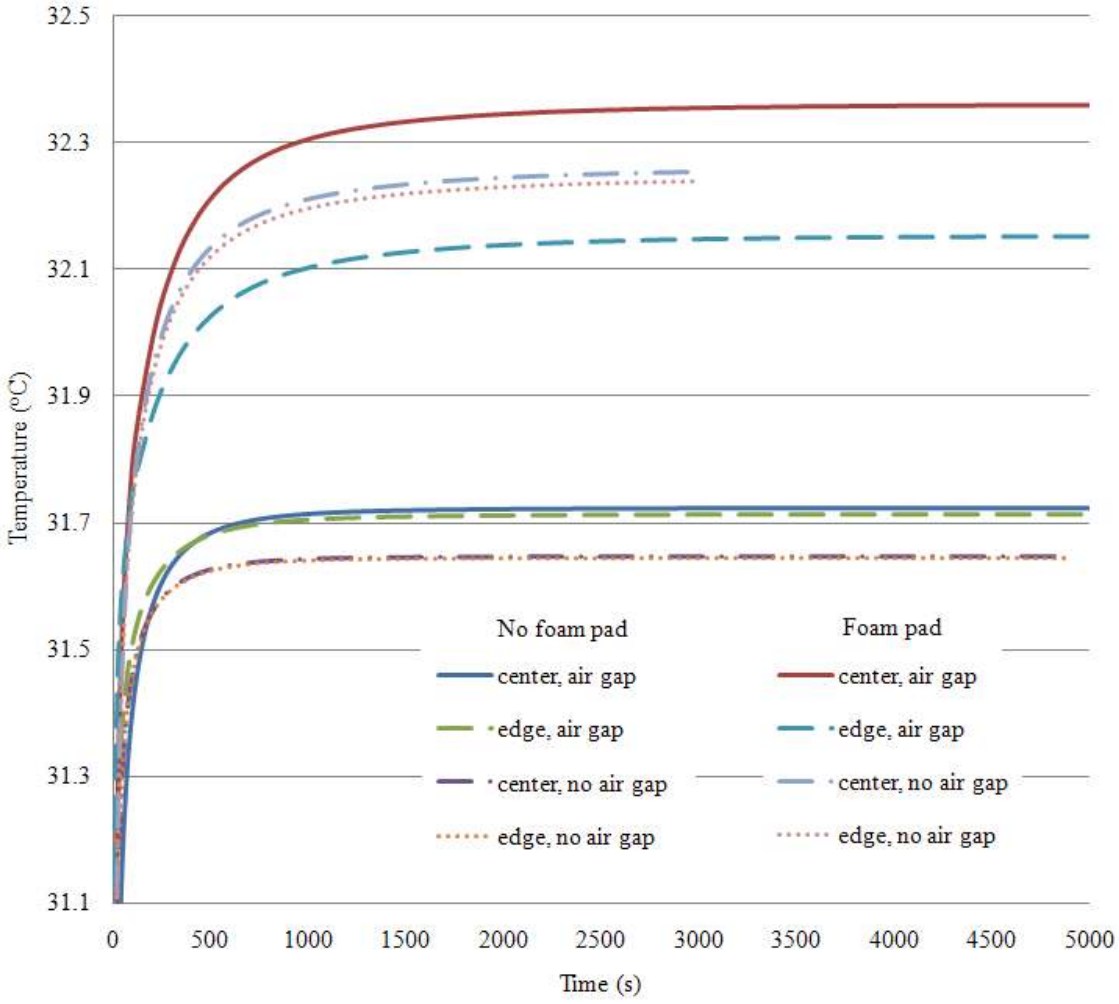

Figure 5.7 Comparison of temperature variations for the cases of measurement with the foam pad and the cases without the foam pad with k = 0.03 W/m-^{o}C.

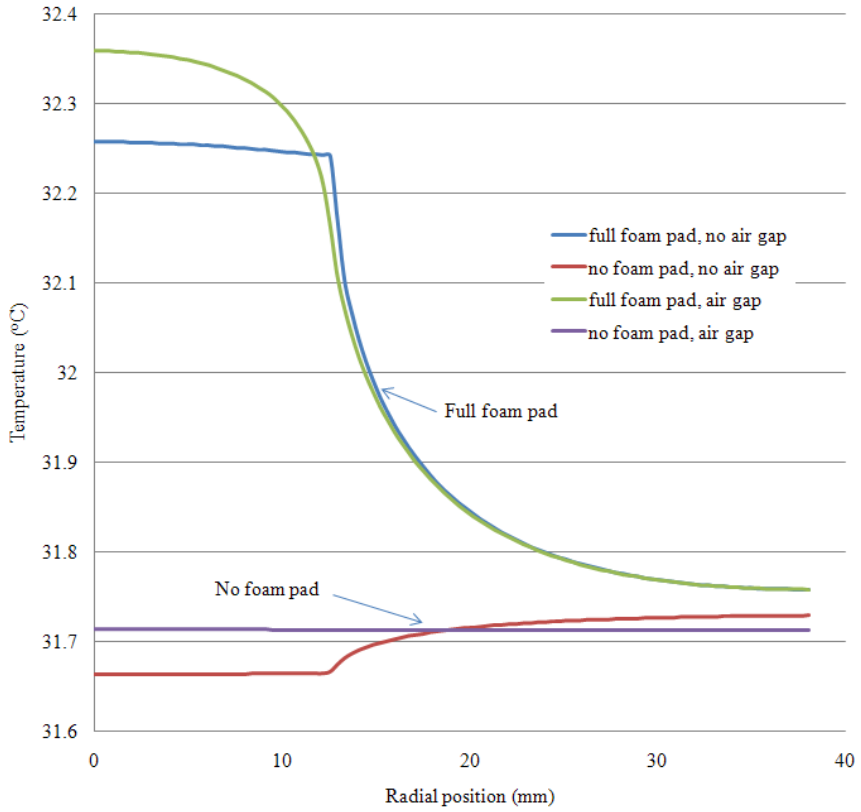

Fig. 5.8 Steady-state skin-surface temperature distributions for the foam pad with k = 0.03 W/m-^{o}C and without the foam pad.

Figure 5.8 shows the skin-surface temperature profiles at steady state for several of the cases considered here. It is quite clear that the contact resistance between the temperature-measuring device and the skin surface is advantageous in maintaining temperature uniformity over the surface of the skin. Removing the foam will assure that a clinical practitioner who uses such a sensor will read the true skin-surface temperature.

CHAPTER 6

CONCLUSION

In Chapter 2, the skin-temperature measurement errors were analyzed for different configurations of the foam pad and for different values of blood perfusion rate. The width of the solution domain was tested. First, a steady state approach was used to test the sensitivity of the solution to the blood perfusion rate ω_b. The results clearly demonstrated that the value of the blood perfusion rate didn't affect the magnitude of the temperature measurement error. Then, different values of thermal conductivity, *k*, for the foam pad were tested. It was shown that the lower the values of k, the less uniform the skin-surface temperature profile, therefore, the larger the error underneath the foam pad. The error magnitude for the most realistic value of k=0.03 W/m-^{o}C was found to be 0.5^{o}C. This value may be regarded as unacceptable. A solution to this problem, which was tested in Chapter 4, was to remove the foam pad and analyze the error.

A transient study of the temperature distribution is discussed in Chapter 3. The time it takes for the steady-state to be achieved was evaluated. Since the value of the blood perfusion doesn't affect the measurement error, a value of $\omega_b = 0.003$ $(m^3/s)/m^3$ was used for the rest of the simulations. As the initial condition of the transient study, the steady-state results of skin, fat, muscle assembly without sensor were used. Then, at time t = 0, the sensor was placed onto the skin and the heat transfer was simulated. As for the steady-state study, three different values of *k* for the foam pad were tested. It was found

that for $k = 0$ W/m-^{o}C, it takes 4,900 seconds for the temperature to reach steady state compared to the cases of $k = 0.03$ W/m-^{o}C and $k = 0.06$ W/m-^{o}C where it takes 3,000 seconds. Even though the time to reach steady state is less for the most realistic values of $k = 0.03$ W/m-^{o}C and $k = 0.06$ W/m-^{o}C, the actual times are unacceptable in a clinical study.

In Chapter 4, the foam pad configurations were investigated for the transient case. The value of k for the foam pad was again varied parametrically. The nine different configurations for the values of the thermal conductivity and the thickness of the foam pad were tested. The three different thickness of the foam pad correspond respectively to full thickness, half thickness and no foam pad. The case with only the copper heat spreader was found to be the best. The copper heat spreader actually lowers the temperature of the skin underneath the sensor, but the error is less than all the previous cases combined. It can be explained by the fact that the copper conducts the heat away from the skin.

In Chapter 5, a contact resistance between the skin surface and the temperature sensor was added to the analysis. The contact resistance was modeled as a thin air gap between the skin surface and the sensor. It was found that in presence of the full foam pad and air gap, the error is greater than without air gap. The best configuration was found to be the sensor without the foam pad, and in presence of an air gap was actually advantageous.

REFERENCES

[1] J. Colin, J. Timbal, Y. Houdas, C. Boutelier, and J.D. Guieu, "Computation of mean body temperature from rectal and skin temperatures," *J Appl Phsyiol*, **31**, pp. 484-489, 1971.

[2] Y. Houdas and E. Ring, "Human body temperature." New York: Plenum Press, 1982, pp. 95-102.

[3] Y. Aoyagi, T.M. McLellan, and R.J. Shephard, "Determination of body heat storage: how to select the weighting of rectal and skin temperatures for clothes subjects," *International Archives of Occupational and Environmental Health (Historical Archives)*, **68**, pp. 325-336, 1996.

[4] A.L Vallerand, G. Sauvourey, A.-M. Hanniquet, and H.M. Bittel, "How should body heat storage be determined in humans: by thermometry and calorimetry?," *European Journal of Applied Physiology (Historical Archive*), **65**, pp. 286-294.

[5] "Glossary of terms for thermal physiology. Third edition. Revised by The Commission for Thermal Physiology of the International Union of Physiological Sciences (IUPS Thermal Commission)," *Journal of Thermal Biology*, **28**, pp. 75-106, 2003.

[6] A.C. Burton, "Human Calorimetry: II. The average temperature of the tissue of the body," *J Nutr*, **9**, pp. 261-280, 1935.

[7] J. Snellen, "Mean body temperature and the control of thermal sweating," *Acta Physiol Pharmacol Neerl*, **14**, pp. 99-174, 1966.

[8] S.D. Livingston, "Calculation of mean body temperature," *Can J Physiol Pharmocol*, **46**, pp. 15-17, 1968.

[9] Y. Aoyagi, T.M. McLellan, and R.J. Shephard, "Determination of body heat storage in clothing: calorimetry versus thermometry," *European Journal of Applied Physiology (Historical Archive)*, **71**, pp. 197-206, 1995.

[10] P. Webb, "Heat storage and body temperature during cooling and rewarming," *Eur J Appl Physiol Occup Phsyiol*, **66**, pp. 18-24, 1993.

[11] A.L. Vallerand, G. Savourey, and J.H. Bittel, "Determination of heat debt in the cold: partitioned calorimetry vs. conventional methods," *J Appl Physiol*, 72, pp. 1380-1385, 1992.

[12] Sparrow, E.M., and Bieberich, M., Personal Communication

[13] Fox, R.H., and Solman, A.J., 1971, "A New Technique for Monitoring the Deep Body Temperature in Man from the Intact Skin Surface," J. Physiol., **212**, pp. 8P-10P.

[14] Fox, R.H., Solman, A.J., Isaacs, R., Fry, A.J., and McDonald, I.C., 1973, "A New Method for Monitoring Deep Body Temperatures from the Skin Surface, Clin. Sci., **44**, pp. 81-86.

[15] Kobayashi T., Nemoto, T., Kamiya, A., and Togawa, T., 1975, "Improvement of Deep Body Thermometer for Man," Ann. Biomed. Eng., **3**, pp. 181-188.

[16] Fox, R.H., and Solman, A.J., 1976, Temperature Measurement, United States Patent 3,933,045.

[17] Muravchick, S., 1983, "Deep Body Thermometry During General Anesthesia," Anesthesiology, **58**, pp. 271-275.

[18] Matsukawa, T., Sessler, D.I., Ozaki, M., Hanagata, K., Iwashita, H., and Kumazawa, T., 1997, "Comparison of Distal Oesophageal Temperature with 'Deep' and Traceal Temperatures," Can. J. Anesth., **44**, pp. 433-438.

[19] Yamakage, M. and Namiki, A., 2003, "Cellular Mechanisms of Airway Smooth Muscle Relaxant Effects of Anesthetic Agents," J. Anesth., 17, pp. 251-258.

[20] Brajkovic, D., and Ducharme, M.B., 2005, "Confounding Factors in the Use of the Zero-Heat-Flow Method for Non-Invasive Muscle Temperature Measurement," Eur. J. Appl. Physiol., **94**, pp. 386-391.

[21] Szlyk, P.C., Sils, I.V., Ferguson, J.D., Matthew, W.T., and Hubbard, R.W., 1986, "Evaluation of Insulated Miniature Thermistors for Skin Temperature Measurement in the Rat," Army Research Institure of Environmental Medicine, Natick, MA, August 1986.

[22] Krause, B.F., 1993, "Accuracy and Response Time Comparisons of Four Skin Temperature-Monitoring Devices, Nurse Anesth., **4**, pp. 55-61.

[23] Burnham, R.S., McKinley, R.S., and Vincent, D.D., 2006, "Three Types of Skin-Surface Thermometers: a Comparison of Reliability, Validity, and Responsiveness," Am. J. Phys. Med. Rehabil., **85**, pp. 553-558.

[24] Pennes, H.H., 1948, "Analysis of Tissue and Arterial Blood Temperatures in the Resting Human Forearm," Journal of Applied Physiology, **1**, pp. 93-122.